

Studies in Random Geometries: Hyper-Cubic Random Surfaces and Simplicial Quantum Gravity

Dissertation

zur Erlangung des Doktorgrades
der Fakultät für Physik
der Universität Bielefeld

vorgelegt von
Sven Bilke

November 1997

Abstract

We analyze two models of random geometries : planar hyper-cubic random surfaces and four dimensional simplicial quantum gravity.

We show for the hyper-cubic random surface model that a geometrical constraint does not change the critical properties of the model compared to the model without this constraint. We analyze the phase diagram for the model with extrinsic curvature.

For four dimensional simplicial quantum gravity we find that in the large volume limit the leading contribution to the entropy does not depend on the underlying topology. We find for the first time a strong back-reaction of the geometric sector for matter coupled to gravity.

Contents

1	Introduction	3
1.1	Discrete random geometries	4
1.2	Random walk	5
1.3	Random surface	7
1.4	Quantum gravity	9
1.5	Matrix models	11
1.6	Branched Polymers	14
1.7	Monte Carlo methods	15
2	Hyper-cubic random surfaces	17
2.1	Introduction	17
2.2	The model	19
2.3	Universality	21
2.3.1	Old method	21
2.3.2	The Baby universe method	22
2.3.3	Discussion	26
2.4	Hyper-cubic random surfaces with extrinsic curvature	27
2.4.1	Introduction	27
2.4.2	Numerical results	29
2.4.3	Discussion	32
2.5	The Algorithm	34
2.5.1	Verification	36
3	Four dimensional simplicial quantum gravity	40
3.1	Introduction	40
3.2	Simplicial quantum gravity	41
3.3	Topology	46
3.3.1	Introduction	46
3.3.2	Model and methods	46
3.3.3	Numerical results	49
3.3.4	Discussion	53
3.4	Simplicial quantum gravity coupled to gauge matter fields	54
3.4.1	Introduction	54
3.4.2	The model	55
3.4.3	The strong coupling expansion	56
3.4.4	Numerical results	59

3.4.5	Discussion	62
3.5	Algorithm	64
3.5.1	Move 15, 51	66
3.5.2	Move 24, 42	68
3.5.3	Move 33	69
4	Summary	70
4.1	Acknowledgement	71

Chapter 1

Introduction

At the beginning of this century two theories forced a new understanding of physics. Quantum theory on the one hand describes the physics on small scales, where "small" scales do not only appear on the atomic level but also for macroscopic objects, such as white dwarfs or super-fluid Helium. On the other hand we have general relativity describing large distance physics which is dominated by the gravitational field.

As of today all attempts to unify these formalisms failed. This is very unfortunate because with such a theory at hand it may be possible to overcome a weak point of general relativity: it predicts space-time singularities and at the same time breaks down at these singularities. In particular, the Big Bang could have produced anything, as far as classical general relativity is concerned. A theory of quantum gravity on the other hand might be able to produce some boundary conditions that can tell us why the universe looks like it does.

It is however very difficult to construct such a theory. The scale in quantum gravity, where quantum effects become important, is set by the Planck mass $M_p \approx 10^{19}$ GeV. Typical energies in particle physics experiments are, however, several orders of magnitude smaller, which is why no experimental results for quantum effects of gravity are available. Therefore one has no no guidance from experiments, which, for example, in the case of the standard model provided very important insight necessary to construct the theory.

String theories are one attempt to unify the fundamental interactions in nature (see for example [1]). These theories avoid the singularities which usually plague quantum field theories by considering the propagation of strings rather than point like particles. Differently from point particles which propagate along paths strings propagate along the world-sheet, a two dimensional surface. It is very interesting that string theories contain spin 2 particles, i.e. gravitons, which makes them a promising candidate for quantum gravity.

General Relativity and string theory have in common that they both are in a certain sense geometric theories. General relativity describes gravity as a curved four dimensional space time metric, strings propagate along two dimensional surfaces. As we will describe in more detail below quantum gravity and quantum string theory both can be looked at as a statistical system of geometries, random geometries. Such systems are, unfortunately, very difficult to deal with analytically,

although some success has been made in two dimensions for random surfaces. However, when coupled to matter with central charge $c \geq 1$ these methods break down. Some observables like the intrinsic Hausdorff dimension are not accessible at all by analytic methods. In higher dimensions almost nothing is known analytically. The motivation of many of the conjectures and assumptions used for higher dimensional models is therefore derived from the experience obtained from the two-dimensional models.

This work addresses these issues. We consider two models with different internal local dimension, two and four. These models are namely hyper-cubic random surfaces, a discretization of bosonic strings, and four dimensional simplicial quantum gravity. To strengthen the common bases for the two models we discuss the subject in a somewhat broader context in the remaining part of this chapter. The motivation and definition of the models, considered in the numerical part of this work, is given in chapters 2 and 3.

1.1 Discrete random geometries

Random geometries have attracted a lot of interest since it was realized that surfaces and higher dimensional manifolds are central to the understanding of the fundamental interactions in nature. In this thesis we are interested mainly in quantum gravity and string theory, but they are also of interest in other fields like biology [2] or condensed matter physics [3]. All of these theories have in common that they describe statistical systems where we have to integrate over geometries.

The thermodynamic properties of these models can be analyzed using standard methods of the theory of critical phenomena. It is generally believed that critical phenomena may play a similarly important role for random geometries as they do in statistical field theory. There it is known that close to a phase transition a certain degree of universality emerges in the sense that models with very different microscopic interaction exhibit the same critical behavior, described by a set of critical exponents. This is usually related to some common symmetry. Something similar happens for two dimensional quantum gravity coupled to matter with central charge $c < 1$. It was shown [4] for this type of models that the entropy exponent γ depends only on the central charge but not on the type of the matter coupled to gravity¹. In higher dimensions one numerically observes universal behavior in the sense that some phases of very different models have similar geometrical properties. For example both types of models considered in this thesis have a phase where the geometry is essentially described by a branched polymer.

Discretization is a very useful tool in analyzing statistical field theories. It reduces the number of degrees of freedom from non-countable to countable. A discrete lattice can serve as a regulator for UV-divergences and also opens the possibility for non perturbative approaches, such as numerical simulations. Typically, models of random geometries are invariant under coordinate transformations. Any regulation of the theory has to obey this invariance. Obviously the regulator introduced by discretizing on the geometric level is reparametrization invariant as this procedure

¹The definition of the exponent γ is given in section 1.3.

does not refer to any coordinate system. However, one has to ask the question what happens to diffeomorphism invariance, the basic symmetry of general relativity, in a discrete space. When taking the continuum limit of the discretized theory one has to check that this symmetry is restored, at least on large distances.

Discretization can also help to define a measure. When performing the integration over distinct physical states for the partition function the measure has to be chosen so as not to over-count surfaces by counting different parameterizations of the same geometry. For two dimensional quantum gravity it was shown that the critical behavior of the discrete dynamical triangulation model (a comprehensive introduction can be found in [5]), where the integral over geometries involving the measure is replaced by a sum over triangulations, and the critical behavior of the continuum theory agree.

The key ingredient that allows to go back from the discrete model to the continuum is universality. If the discretized model is in the same universality class with the continuous version its critical properties describe continuum physics. The physical reason is that if the correlation length in units of lattice spacings diverges, for example at a second order phase transition, details of the discretization become unimportant and the system exhibits continuum behavior.

1.2 Random walk

A random walk describes the propagation of a point like particle in d - dimensional space. Despite its relative simplicity it contains many of the aspects common to other random geometries. As this model is well known also to readers from outside this field of research, it is perfect to demonstrate these aspects. For the details of the calculations we refer to [6].

In a quantum theory the amplitude $G(x, x')$ for a particle to go from x to x' is given by the sum over all possible trajectories $P_{xx'}$ connecting these points. In Euclidean space we have

$$G(x, x') = \int_{P_{xx'}} \mathcal{D}P \exp(-S[P_{xx'}]), \quad (1.1)$$

where $S[P_{xx'}]$ is the classical action for the given path. As such we choose the simplest characterization of the path, its length:

$$S = m_o \int dl = m_0 \int_0^1 d\xi \sqrt{\partial x_\mu \partial x_\mu}. \quad (1.2)$$

In the right-hand expression we introduced a parametrization

$$x(\xi) : [0, 1] \rightarrow R^D, x(0) = x, x(1) = x' \quad (1.3)$$

of the path. Expression (1.2) is invariant under reparametrizations given by

$$x_\mu(\xi) \rightarrow x_\mu(\phi(\xi)) \quad (1.4)$$

with the function $\phi(\xi)$ satisfying the conditions

$$\phi(0) = 0, \quad \phi(1) = 1, \quad \frac{d\phi(\xi)}{d\xi} > 0. \quad (1.5)$$

We will show that with the action (1.2) the quantum amplitude (1.1) describes the propagation of a free relativistic particle. Other terms in the action, for example higher derivative terms, can be relevant in the continuum as well. A non-trivial term is for example a coupling to the external curvature K .

$$\epsilon \int dl |K| \quad (1.6)$$

For finite coupling ϵ one finds the critical behavior of the ordinary random walk discussed below. In the limit $\epsilon \rightarrow \infty$ one finds a different class, smooth random walks [7, 8].

The expression (1.1) is rather formal. The measure $\mathcal{D}P$ has to be defined in such a way that the integral counts only the number of distinct paths, i.e. paths which differ only by reparametrization (1.4) have to be counted only once. In continuum formulations one formally defines this as the number of all paths modulo reparametrizations,

$$\mathcal{D}P \rightarrow \frac{\mathcal{D}P}{\mathcal{D}f}. \quad (1.7)$$

A way to define the measure and at the same time regularize the model is to discretize it. This has to be done carefully, though: it is surely wrong to cut the interval $0 \leq \xi \leq 1$ into equally small pieces, as this would spoil reparametrization invariance. Instead of discretizing a certain parameterization one has to discretize the internal structure of the path. This amounts to considering only piecewise linear paths where each step on the path is of length a , i.e. we refrain from discussing structures smaller than a . This cut-off is invariant by definition. The possible length of the path is now $l = na$ and the action is $S = m_0 l$. With this discretization the expression for the amplitude (1.1) is

$$G_a(x, x'; m_0) = \sum_{n=1}^{\infty} \exp(-m_0 a n) \int \prod_{i=0}^n d\vec{e}_i \delta\left(a \sum \vec{e}_i - (x - x')\right), \quad (1.8)$$

where the integral is over unit-vectors in R^d . After Fourier transforming this and some algebra one finds

$$G_a(p; m_0) = \frac{1}{1 - \exp(-m_0 a) f(pa)} \quad (1.9)$$

with

$$f(pa) = \int d\vec{e} \exp(-ip\vec{e}) \approx f(0)(1 - c^2(pa)^2 + \dots). \quad (1.10)$$

To recover the continuum from the discrete description the lattice spacing has to go to zero: $a \rightarrow 0$. One gets the propagator for the free relativistic particle if at the same time the bare mass m_0 is renormalized such that

$$\exp(-m_0 a) f(pa) \rightarrow 1 - c^2 m_{ph}^2 a^2, \quad \text{i.e.} \quad m_0 = \frac{\log(f(0))}{a} + c^2 m_{ph}^2 a, \quad (1.11)$$

where m_{ph} is the physical mass. Putting the last three formulas together one gets

$$G_a(p; m_0) \rightarrow \frac{1}{c^2 a^2} \frac{1}{p^2 + m_{ph}^2} = \frac{1}{c^2 a^2} G_c(p; m_{ph}) \quad (1.12)$$

when one collects the leading order a^2 terms. The discrete amplitude G_a in this limit is related to the continuum propagator G_c of the free relativistic particle by the divergent factor $\frac{1}{c^2 a^2}$, which can be interpreted as a wave function renormalization.

It is interesting to note that these results are quite universal. They do not depend on the details of the discretization. For example one finds the same continuum limit for the random walk on a discrete lattice Z^D , where one has to sum over unit-vectors of Z^D in (1.1) rather than integrating over the unit-sphere. One also finds universality concerning the action. Consider for example the covariant action of one dimensional gravity :

$$S[x, g] = \frac{1}{\alpha} \int_0^1 d\xi \sqrt{g(\xi)} \left[g^{ab}(\xi) \frac{\partial x^\mu}{\partial \xi^a} \frac{\partial x^\mu}{\partial \xi^b} + \mu \right], \quad (1.13)$$

where an independent internal metric "tensor" g_{ab} , $a = b = 1$ has been introduced. The partition function

$$Z = \int \frac{\mathcal{D}[g]}{\mathcal{D}f} \mathcal{D}x e^{-S[x, g]}. \quad (1.14)$$

contains in this case an integration over equivalence classes of metrics. The classical equations of motion obtained from (1.13) by variation of g_{ab} and x independently agree with those one gets from the action (1.2). But it is a non-trivial observation that they agree on the quantum level because in principle the metric field could induce different quantum anomalies.

1.3 Random surface

While point particles propagate along path a string sweeps out a surface when propagating. It is natural to expect that the generalization of the quantum amplitude (1.1) to surfaces describes the propagation of a free relativistic string if one chooses similar to (1.2) an action proportional to the area of the surface. Higher derivative terms, like curvature-squared terms or extrinsic curvature terms may also be relevant in a possible continuum limit. It is, however, best to start with a simple action and check the relevance of other terms only afterwards.

One such action is the Nambu-Goto action

$$S_{NG}[S(l_i)] = \mu \int_{S(l_i)} dA = \mu \int_{M(l_i)} d^2 \xi \sqrt{\left(\frac{\partial x^\mu}{\partial \xi^1} \right)^2 + \left(\frac{\partial x^\mu}{\partial \xi^2} \right)^2 - \left(\frac{\partial x^\mu}{\partial \xi^2} \frac{\partial x^\mu}{\partial \xi^1} \right)^2}. \quad (1.15)$$

The metric of the surface is completely determined by the embedding of the surface x^μ into a D -dimensional space. The 2-loop quantum amplitude is

$$G(l_1, l_2) = \int_{s_{l_1, l_2}} \mathcal{D}\mathcal{S} \exp(-S[S_{l_1, l_2}]), \quad (1.16)$$

where the integration extends over all surfaces S_{l_1, l_2} which have l_1 and l_2 as a boundary.

The non-polynomial action (1.15) makes the analytic treatment of the Nambu-Goto string very difficult. Therefore Polyakov suggested [9] a different string model. He introduced an internal metric g_{ab} , $a, b = 1, 2$ which is independent of the embedding. The action for this model is:

$$S[g, x] = \alpha \int_{M(l_i)} d^2\xi \sqrt{g} \left[g^{ab} \frac{\partial x^\mu}{\partial \xi^a} \frac{\partial x^\mu}{\partial \xi^b} + \mu \right]. \quad (1.17)$$

The 2-loop Greens function now also integrates over the g_{ab} modulo reparametrizations :

$$G(l_1, l_2) = \int_{s_{l_1, l_2}} \frac{\mathcal{D}g_{ab}}{\mathcal{D}f} \int \mathcal{D}_g x \exp(-S[g, x]). \quad (1.18)$$

The partition function for fixed area A is

$$Z(A) = \int_s \frac{\mathcal{D}g_{ab}}{\mathcal{D}f} \int \mathcal{D}_g x e^{-S[g, x]} \delta \left(\int d^2\xi \sqrt{g} - A \right). \quad (1.19)$$

We define the entropy exponent γ by the asymptotic behavior of the partition function for large A ,

$$Z(A) \approx e^{\mu_c A} A^{\gamma-3}, \quad (1.20)$$

where μ_c is the critical coupling of the model.

The classical equations of motion derived from the actions (1.15) and (1.17) agree because in the saddle point solution the metric g_{ab} takes the form induced by the embedding. But it is not at all obvious that the quantum theories are identical. It has been demonstrated [10] that the two quantizations are equivalent in the critical dimension $D = 26$. In lower dimensions it is not clear that the quantization 'based' on the two actions are indeed the same. It is, for example, not excluded that the $c = 1$ barrier, which we discuss below, is absent for the model defined by (1.16).

In defining a string theory using the the Polyakov action one has to deal with the problem of avoiding over-counting of surfaces. The measure

$$\frac{\mathcal{D}g_{ab}(\xi)}{\mathcal{D}f(\xi)} \quad (1.21)$$

is a functional integral over the space of metrics divided by the volume of the diffeomorphism group. In the continuum one can deal with this problem by gauge fixing. In the conformal gauge the metric g_{ab} can be written as

$$g_{ab} = e^\sigma \delta_{ab} \quad (1.22)$$

with only one parameter σ . A naive argument which explains this result is that the four components of the metric tensor are not independent; a metric tensor is symmetric, i.e. the off-diagonal elements are identical. Reparametrization invariance kills another two degrees of freedom, so one ends up with only one free parameter. This, however, is a bit too naive because the conformal gauge is accessible only if

the required coordinate transformation is non singular. It can be shown [9] that on a sphere this is always the case.

The action in (1.19) is invariant under the conformal deformation $g_{ab}(\xi) \rightarrow e^{\sigma(\xi)}g_{ab}(\xi)$ of the metric. Therefore the classical action does not depend on σ in the conformal gauge which reflects the triviality of the classical model. In the quantum theory, however, the measure $\mathcal{D}_g x$ transforms in a non-trivial way. This so-called conformal anomaly brings back the σ dependence into the the effective action

$$S_l[\phi] = -\frac{D}{48\pi} \int d^2z (2\partial_z \sigma \partial_{\bar{z}} \sigma + \mu^2 e^\sigma), \quad (1.23)$$

which is known as Liouville action. The gauge-fixing of the measure $\mathcal{D}g$ introduces a ghost $\frac{26}{D}S_l$. The partition function for the Polyakov string in the conformal gauge is :

$$Z = \int \mathcal{D}\sigma \exp \left\{ -\frac{26-D}{48\pi} \int d^2z (2\partial_z \sigma \partial_{\bar{z}} \sigma + \mu^2 e^\sigma) \right\}. \quad (1.24)$$

The x^μ in the Polyakov action (1.17) can be interpreted as D scalar fields coupled to the surface described by the metric g_{ab} . Note that with this interpretation the case $D = 0$, a surface embedded into a zero dimensional space, does make sense. In section 1.4 we will show that this case describes pure gravity without matter. In [4] it was shown that the entropy exponent γ for two dimensional quantum gravity coupled to conformal matter with central charge c is given by

$$\gamma = \frac{c-1-\sqrt{(1-c)(25-c)}}{12}. \quad (1.25)$$

The central charge c in a sense counts the number of degrees of freedom of the conformal field theory. For a free bosonic strings it can be identified with the dimension of the embedding space. If one considers only unitary models with $c < 1$ the exponent γ takes only a discrete set of negative values

$$\gamma = -\frac{1}{m}, m = 2, 3, \dots \quad (1.26)$$

Note that the formula (1.25) is not valid for $c > 1$ because it gives unphysical complex results; in the literature this is often referred to as the " $c = 1$ barrier". A more detailed discussion can be found in section 2.1.

1.4 Quantum gravity

The classical description of gravity is given by Einsteins theory of general relativity (for an introduction see for example [11, 12]). The space-time metric describes the gravitational field. The field equations for the metric field are given by

$$R_{ik} - \frac{1}{2}g_{ik}R = \frac{8\pi G_N}{c^4}T_{ik}. \quad (1.27)$$

where $G_N = 6.6710^{-11}\text{m}^3\text{kg}^{-1}\text{s}^{-2}$ is Newton's constant, g_{ik} the metric tensor and T_{ik} the energy-momentum tensor of a matter field coupled to gravity. The Ricci

tensor R_{ik} and the scalar curvature $R = g_{ik}R^{ik}$ are functions of the metric tensor and contain first and second derivatives. The dynamical variable of the theory is the metric of space time.

The classical equations of motion for this metric can be derived using the principle of least action, from the classical action. It is generally believed that it is possible to define a quantum theory of gravity using the path integral formalism. One assumes that not only the classical trajectory but all trajectories weighted by $e^{-S[g]}$ contribute to quantum mechanical transition probabilities, giving

$$\langle g^{(f)} | g^{(i)} \rangle \propto \int_{g^{(i)} \rightarrow g^{(f)}} \frac{\mathcal{D}[g]}{\mathcal{D}f} e^{-S[g]}. \quad (1.28)$$

The integral is over all D -dimensional Euclidean space time metrics which satisfy the boundary conditions $g^{(f)}, g^{(i)}$. As usual in quantum field theory one has to switch to the Euclidean formulation. Unlike for conventional field theories it is still an open issue whether the Minkowski formulation can be recovered by a Wick rotation [13]. In $D \leq 4$ dimensions the action in Euclidean space has the form

$$S = \frac{1}{G_N} \int d^D \xi \sqrt{|g|} (2\Lambda - R) + S_{Matter}, \quad (1.29)$$

where we have introduced the cosmological constant Λ .

The quantum amplitude (1.28) describes a system of random geometries. We define the partition function of quantum gravity by

$$Z = \int \frac{\mathcal{D}[g]}{\mathcal{D}f} e^{-S[g]}. \quad (1.30)$$

The case $D = 1$ has already been discussed in the context of random walks (1.14). The distance $l = \int \sqrt{|g|} d\xi$ is an invariant internal characteristic of the metric, but we cannot define an internal curvature. Therefore the scalar curvature R term in (1.29) drops out. Comparing with the action (1.13) we see that the two expressions differ by the term

$$S[x, g] = \frac{1}{\alpha} \int_0^1 d\xi \sqrt{g(\xi)} \left[g^{ab}(\xi) \frac{\partial x^\mu}{\partial \xi^a} \frac{\partial x^\mu}{\partial \xi^b} \right], \quad (1.31)$$

which describes the embedding of the random walk in a Δ -dimensional space. For gravity it does not make sense to interpret the $x^\mu, \mu = 1, \dots, \Delta$ as an embedding, but one can interpret this term as the contribution of Δ scalar fields. The case $\Delta = 0$, i.e. the random walk embedded in a zero dimensional space, describes one dimensional quantum gravity without matter fields.

For $D = 2$ quantum gravity is described by the Polyakov string (1.18) embedded in zero dimensions. Note that for surfaces the curvature R is a local invariant, so we have a new degree of freedom compared to the one dimensional model. On the other hand it is known from the Gauss-Bonnet theorem,

$$\oint d^2 \xi \sqrt{|g|} R = 4\pi \chi_E, \quad (1.32)$$

that the integrated curvature is a topological invariant with $\chi_E = 2 - 2h$, where h is the number of handles in the surface. The Euler character is $\chi_E = 2$ for the sphere, $\chi_E = 0$ for a torus and so on. For fixed topology the curvature term in the action (1.29) gives therefore no dynamical contribution, which makes the classical model trivial. One might suspect that this is also the case for the quantum model. In fact the two dimensional model does not contain gravitons, however the conformal quantum-anomaly generates the non-trivial behavior discussed in the previous section.

Quantum gravity in physical four dimensions is one of the models considered in the numerical part of this work. Therefore we discuss this case in detail in chapter 3. Here we only want to mention that for the time being no continuum solution for the model is known. The discrete approach, which is very successful in two dimensions can be generalized to four dimensions. With this method at hand numerical simulations allow us to survey properties of quantum gravity in this interesting case.

1.5 Matrix models

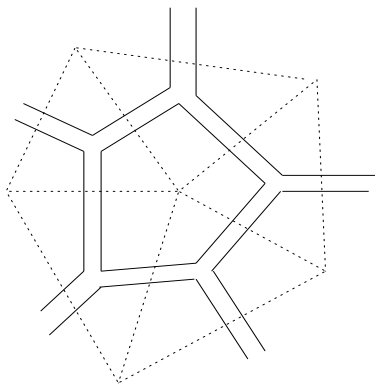


Figure 1.1: A part of a M^3 -Graph. The dotted line depicts the triangulation dual to the graph.

In dynamical triangulations [14, 15, 16], the path integral (1.30) over two dimensional equivalence classes of metrics is replaced by a sum over triangulations T :

$$\int \frac{Dg_{ab}}{Df} \rightarrow \sum_T \frac{1}{\sigma(T)} \quad (1.33)$$

The symmetry factor $\sigma(T)$ is a discrete remnant of the reparametrization group. It is mainly important for small triangulations because typically larger triangulations are not symmetric. A triangulation is a surface obtained by gluing together equilateral triangles along their edges so that exactly two triangles meet on each edge with possible exceptions on the boundary. As in the continuum we choose the action to be proportional to the area. In the discrete model the area is given by the number n of triangles in the triangulation.

In the partition function

$$Z(\mu, G) = \frac{1}{\sigma} \sum_{\mathcal{T}} \exp(-\mu n) = \sum_{\chi} \exp \frac{\chi}{G} \sum_n \exp(-\mu n) \mathcal{N}_{\chi}^{(c)}(n). \quad (1.34)$$

the topology is not a priori fixed. However the number of graphs with free topology grows factorially with n and therefore the naive topological expansion in the number h of holes in the surface is as stands ill defined. Therefore calculations and numerical simulations are in most cases done for ensembles with fixed topology. At the end of this section we discuss the double scaling limit, which can be used to define the model with coherent contributions from all topologies.

The dynamical triangulations model can be formulated as a matrix model, defined by the generating function

$$\bar{Z} = \log \int dM \exp(-Tr M^2 + \frac{g}{\sqrt{N}} Tr M^3), \quad (1.35)$$

where M is a $N \times N$ hermitian matrix and dM the flat measure

$$dM = \prod_{i=1}^N dM_{ii} \prod_{1 \leq i < j \leq N} d(Re M_{ij}) d(Im M_{ij}). \quad (1.36)$$

Doing perturbative expansions in g one gets Feynman diagrams similar to those depicted in figure 1.1. Note that the dual graph, drawn in dotted lines, is a triangulation. Because (1.35) generates all possible graphs it sums over all triangulations. It should be emphasized that the results presented below do not rely on using triangulations. In [17] it was shown that the continuum limit for the model with a lattice built from squares, pentagons, etc. agrees with the result obtained for triangulated surfaces.

Differently from a standard Feynman graph, the propagator

$$\langle M_{ij} M_{kl}^* \rangle = \delta_{il} \delta_{jk} = \begin{array}{ccc} i & \longrightarrow & l \\ j & \longleftarrow & k \end{array}$$

carries two indices. This is necessary to interpret the graph as a two dimensional surface; a priori Feynman graphs do not have any "dimension". Moreover, (1.35) generates orientable surfaces because M is hermitian. Due to the Wick theorem one gets the n th term of the perturbative expansion by summing over all diagrams with n vertices, where each vertex has a weight

$$\frac{g}{\sqrt{N}} \Phi_{ij} \Phi_{jk} \Phi_{ki} = \begin{array}{c} \begin{array}{ccc} & i & \\ & \nearrow & \\ i & \longleftarrow & \\ j & \longrightarrow & \\ & \searrow & \\ & k & \end{array} \\ \cdot \end{array} \quad (1.37)$$

A closed index loop contributes a factor N because the trace sums over the indices of the matrix. A diagram D with $V = n$ vertices, L closed index-loops and P

propagators therefore contributes

$$\frac{1}{\sigma(D)}(gN^{-1/2})^V N^L = g^V \frac{1}{\sigma(D)} N^\chi, \quad (1.38)$$

where σ is the symmetry factor of the diagram. The expression on the right hand side is obtained by noting $3V = 2P$ and using the Euler theorem $V + P - L = 2 - 2h = \chi$, where χ is the Euler character of the surface, which uniquely identifies the topology of the graph.

In the diagrammatic expansion the partition function of the one matrix model reads

$$\bar{Z}(g, N) = \sum_h N^\chi \sum_n g^n \sum_{D \in \mathcal{D}_{h,n}} \frac{1}{\sigma(D)} = \sum_h N^\chi \sum_n g^n \mathcal{N}_\chi^{(c)}(n). \quad (1.39)$$

The number $\mathcal{N}_\chi^{(c)}(n)$ of graphs can be calculated with the method of orthonormal polynomials [18], one finds

$$\mathcal{N}_\chi^{(c)}(n) \propto n^{\gamma_\chi - 3} g_c^{-n}. \quad (1.40)$$

The entropy exponent

$$\gamma_\chi - 2 = \bar{c}\chi, \quad \bar{c} = -\frac{5}{4} \quad (1.41)$$

is linear in χ . The constant g_c , the critical coupling, does not depend on the topology.

In the limit $N \rightarrow \infty$, the so-called planar limit, only diagrams with spherical topology $\chi = 2$ contribute to the sum over topologies in the partition function (1.39). Contributions from higher genus diagrams are suppressed by N^{-2h} . On the other hand these contributions are enhanced as $g \rightarrow g_c$, which can be seen from the asymptotic behavior of the partition function with fixed topology :

$$Z_\chi(g) = \sum_n g^n \mathcal{N}_\chi^{(c)}(n) \approx (g - g_c)^{2 - \bar{c}\chi} \quad (1.42)$$

This suggests that if the limits $N \rightarrow \infty$ and $g \rightarrow g_c$ are taken together in a correlated way the large N genus suppression can be compensated by the $g \rightarrow g_c$ enhancement. This would result in a coherent contribution from all genus surfaces [19, 20, 21]. This so-called double scaling limit is defined by taking the limits $N \rightarrow \infty, g \rightarrow g_c$ while holding fixed the the 'renormalized' string coupling

$$\kappa^{-1} = N(g - g_c)^{-\bar{c}}. \quad (1.43)$$

By comparison of (1.39) with the partition function of dynamical triangulations (1.34) we find the relations

$$N = \exp \frac{1}{G}, \quad g = \exp(-\mu) \quad (1.44)$$

for the coupling constants. For spherical topologies we can compare the exponent γ_2 with the the continuum results (1.25). The value $\gamma_2 = -\frac{1}{2}$ obtained from (1.41)

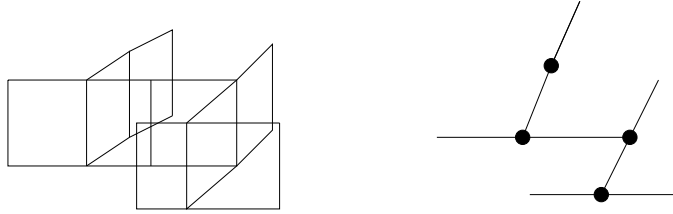


Figure 1.2: A part of a hyper-cubic surface and the representation of the surface as a branched polymer

agrees with the value $\gamma = -\frac{1}{2}$ obtained in the continuum for pure gravity, i.e. $c = 0$. Some variants of the matrix model discussed here can be used to describe discrete gravity coupled to matter. For example a particular two matrix model describes the Ising model ($c = \frac{1}{2}$) coupled to gravity [22]. One finds $\gamma = -\frac{1}{3}$ in this case which is in agreement with the results obtained in the continuum.

1.6 Branched Polymers

Many models of random geometries, for example the two types of models considered in this thesis, have a phase which can essentially be described by branched polymers. Following [6] we want to derive the result $\gamma = 1/2$ for the entropy exponent because we frequently refer to this result. As an example for a branched polymer structure we show in figure 1.2 a small hyper-cubic surface, which can be decomposed into small components by cutting open loops of length two. The individual components are not critical, their size is of the order of the lattice spacing. The only way the number of plaquettes can grow to infinity is by successive gluing of branches, all the dynamics lies in this gluing. This dynamics is described by the branched polymer model : in the right hand side of figure 1.2 the individual components are represented as links l_i with an associated chemical potential μ . We also introduce a weight f_n for the joining of n links l_i at a vertex v_n . The partition function for the branched polymer model is

$$Z(\mu) = \sum_{\text{BP}} e^{-\mu N} \prod_v f_n(v), \quad (1.45)$$

where the sum runs over all branched polymers, i.e. tree graphs if we restrict ourselves to spherical topology. To extract γ we consider the one-point function

$$G(\mu) \approx c(\mu - \mu_c)^{1-\gamma}, \quad (1.46)$$

the amplitude of rooted trees with one marked vertex. Such a tree can be built recursively as seen in figure 1.3, where the blobs represent a rooted tree. This can be used to write down the self-consistent equation [23]

$$G_\mu = e^{-\mu} (1 + f_2 G_\mu + f_3 G_\mu^2 + \dots). \quad (1.47)$$

Solving for e^μ gives :

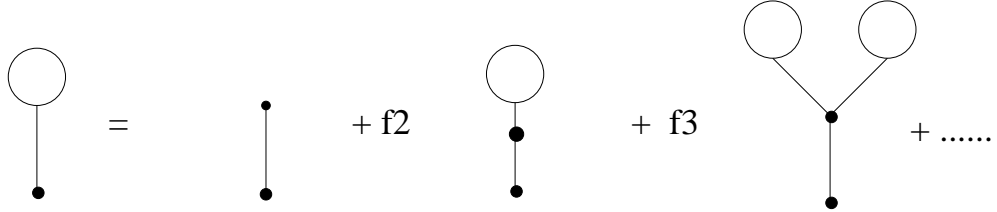


Figure 1.3: The self-consistent equation for rooted trees.

$$e^\mu = \frac{1 + f_2 G_\mu + f_3 G_\mu^2 + \dots}{G_\mu} = F(G_\mu) \quad (1.48)$$

We conclude that the lowest value μ_c of μ for which eq. (1.48) has a solution is the minimum of $F(G_\mu)$ if the weights f_n are positive :

$$\frac{d}{dG_\mu} F(G_\mu)|_{\mu=\mu_c} = 0 \quad (1.49)$$

Therefore the linear term drops out if one expands $(\mu - \mu_c)$ in G_μ :

$$\mu - \mu_c \approx (G_{\mu_c} - G_\mu)^2 \quad \text{i.e.} \quad G_\mu \approx G_{\mu_c} - c\sqrt{\mu - \mu_c}. \quad (1.50)$$

Comparing with eq. (1.46) one finds $\gamma = \frac{1}{2}$.

1.7 Monte Carlo methods

The algorithms used to simulate the two different models, hyper-cubic random surfaces and four dimensional simplicial quantum gravity, are both based on the same numerical technique, namely Monte Carlo methods. We give a detailed description of the algorithms separately for each model in section 2.5 and 3.5. Here we want to summarize briefly some well-known facts about Monte Carlo algorithms which we use as a foundation for the more detailed discussion.

Despite the apparent simplicity of a discrete partition function in the form

$$Z = \sum_{\Gamma} \exp(-S[\sigma]) \quad (1.51)$$

it is only for a few simple systems possible to actually perform the summation. Even with a computer it is only for very small systems possible to sum over *all* states $\sigma \in \Gamma$ because the number of states $\mathcal{N}_\sigma(V)$ in general grows exponentially with the volume. However, only comparatively few states give a significant contribution to the partition function. The overwhelming majority of the σ are either entropically suppressed or damped by the Boltzmann factor $\exp(-S[\sigma])$. Monte Carlo algorithms are a method to sample the important contributions by choosing at random n samples $\sigma_i \in \Gamma$ with the probability distribution

$$\pi(\sigma_i) \propto \exp -S[\sigma_i]. \quad (1.52)$$

This is the thermodynamical equilibrium distribution. One can therefore approximate observables by their expectation value

$$\langle \mathcal{O} \rangle = \frac{\sum_{\{\sigma_i\}} \mathcal{O}(\sigma_i)}{n}. \quad (1.53)$$

It follows from the central limit theorem that the error depends on the number n of measurements as $\sigma(\mathcal{O}) \propto 1/\sqrt{n}$ if the σ_i are independent.

A problem is of course how to choose the σ_i at random from the state space Γ . Dynamical Monte Carlo methods simulate a Markov process which generates a sequence of σ_i . The main ingredient of the Markov chain is a set of transformation

$$\sigma_i \rightarrow \sigma_{i+1} \quad (1.54)$$

and a probability matrix $(\mathcal{P}(\sigma_a, \sigma_b))_{ab}$. One can show that the n -step transition probability $\mathcal{P}^{(n)}(\sigma_a, \sigma_b)$ converges to a equilibrium distribution

$$\lim_{t \rightarrow \infty} \mathcal{P}^{(t)} \rightarrow \pi(\sigma_b) \quad (1.55)$$

if the following conditions are satisfied:

- **Ergodicity** For each pair $\sigma_1, \sigma_2 \in \Gamma$ exists a sequence of transformations which as a whole transform σ_1 into σ_2 .
- **Stationarity** The following equation holds for the components of the transition matrix and for all $\sigma_b \in \Gamma$:

$$\sum_{\sigma_a} \pi(\sigma_a) \mathcal{P}(\sigma_a, \sigma_b) = \pi(\sigma_b) \quad (1.56)$$

The solutions of the detailed balance equation

$$\pi(\sigma_a) \mathcal{P}(\sigma_a, \sigma_b) = \pi(\sigma_b) \mathcal{P}(\sigma_b, \sigma_a) \quad (1.57)$$

satisfy equation (1.56). This condition is stronger than (1.56) but practically more convenient. In praxis the following solutions of this equation are important. With the heat bath weight

$$\mathcal{P}(\sigma_a, \sigma_b) = \pi(\sigma_b) \quad (1.58)$$

the transition probability to the new state σ_b is independent from the old state σ_a . The Metropolis weight accepts all transformation for which $\pi(b) > \pi(a)$. The weight for the inverse transformation can be deduced from (1.57). The shorthand notation for both directions

$$\mathcal{P}(\sigma_a, \sigma_b) = \min \left\{ 1, \frac{\pi(\sigma_b)}{\pi(\sigma_a)} \right\}. \quad (1.59)$$

is especially useful for a computer implementation.

Chapter 2

Hyper-cubic random surfaces

2.1 Introduction

The Nambu-Goto action (1.15) describes a bosonic string embedded in a D dimensional space \mathcal{R} . The world-sheet metric is, different from a theory of quantum gravity using the Polyakov string, completely determined by the embedding of the string in \mathcal{R} . One can therefore attempt to discretize the model by discretizing the embedding space. This idea was used long ago in [24] to define a model of hyper-cubic random surfaces. However, in [25] it was shown that this discretized model is trivial because the surfaces which dominate the partition function have the structure of branched polymers, basically one dimensional highly branched thin tubes. It was generally believed on grounds of renormalization group arguments that one cannot cure this behavior by adding local terms to the action. It therefore came as a surprise when some years later numerical results for a slightly modified model with a local constraint indicated non-trivial behavior [26]. In $D = 4$ the anomalous scaling dimension $\eta \approx 1$ was measured to be different from zero and for the entropy exponent $\gamma \approx 0.25$ was obtained.

In today's language of random surface theory one can interpret this model as a random surface model coupled to matter with central charge $c = D > 1$. The KPZ-formula (1.25) classifies $2d$ -gravity coupled to matter with $c \leq 1$. The $c > 1$ regime however, where (1.25) gives an unphysical imaginary exponent γ , is still not completely understood. Discretized models of $2d$ -gravity are, on the other hand, well defined for $c > 1$. Numerical simulations clearly indicate branched polymer behavior for $c \lesssim 5$, although in the regime $1 < c \gtrsim 5$ the numerical evidence is not so obvious. They seem to indicate a smooth cross-over to the branched polymer phase as c increases. Based on the numerical evidence one might conclude that there is a different critical behavior for $1 < c \lesssim 5$, although it has been argued [28], based on a renormalization group analysis, that the universal behavior for $c > 1$ models is always a branched polymer structure. This behavior, however, is masked by the presence of the $c = 1$ fixed point, which becomes complex for $c > 1$. This would lead to exponentially enhanced finite size effects. A recent numerical work [27] supports this conjecture.

In view of this result $\gamma \approx 0.25$ for the modified hyper-cubic random surface model, considered in [26] is, if true, very interesting [29]. It would provide a very

simple model with a non-trivial value, besides the mean field result $\gamma = \frac{1}{3}$, of the series

$$\gamma = \frac{1}{n}, n = 2, \dots \quad (2.1)$$

of positive γ values discussed by Durhuus [30]¹. However one may ask how a local constraint, which disappears after one coarse graining step in a renormalization group analysis, could influence the large scale properties of the model. On the other hand, it is just the fact that the coarse grained surfaces in general does not belong to the constrained class of surfaces which invalidates the triviality proof [25] for the unrestricted model. In addition a different universal behavior would indicate the breakdown of universality because in a sense the constraint is nothing but a detail of the discretization.

A mechanism which might induce non-trivial behavior into the model is suggested by the renormalization argument used to derive the series (2.1). In this argument the surface is decomposed into shortest loop irreducible components, *i.e.* components which cannot be cut into two parts along a (model dependent) shortest possible loop. For systems with $n > 2$ the entropy of the surface is still dominated by branching. But differently from branched polymers the components of the surface which form the branches are themselves critical with $\bar{\gamma} < 0$. Such a behavior is induced by matter field(s) with the couplings tuned to their critical values. The local constraint introduced into the model (2.5) can be written as an additional term in the action (2.6) as a coupling to a external curvature. For the (actually infinite) coupling, introduced by the constraint, the model could be critical and above scenario could apply.

We will address the question if a local constraint induces really a different critical behavior. We furthermore generalize the unrestricted hyper-cubic random surface model by adding to the action a term coupled to the external curvature of the surface. This model allows an interpolation between the [25] unconstrained and the potentially non-trivial [26] constrained version of the model. In a optimistic scenario one may hope that by tuning the couplings one may induce a non-trivial phase structure with a weak coupling branched polymer phase and a strong coupling flat phase. At the phase transition the model might have a another value of γ , just as in the scenario described by Durhuus.

¹see also section 2.4.1

2.2 The model

A hyper-cubic surface is an orientable surface embedded in Z^D , obtained by gluing pairwise together plaquettes $P_{x,y}$ along their links until no free link is left. A plaquette $P_{x,y}$ is a unit-square which occupies one of the unit-squares $S_z^\mu, \mu = 1 \cdots D$ in the embedding lattice. In the following we use the word square to refer to the embedding lattice and the words link or plaquette to describe the internal connectivity of the surface. A link is shared by exactly two plaquettes, which are glued together along each one of their edges. Note that a link or a square in the embedding lattice can be occupied more than once. In other words, the surface is not self avoiding; touching and self intersection are allowed.

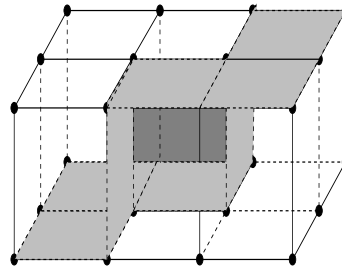


Figure 2.1: A part of a hyper-cubic surface in $D=3$ dimensions

The hyper-cubic random surface model is defined by the partition function:

$$\mathcal{Z}(\beta) = \sum_{E \in \mathcal{S}} e^{-S} = \sum_A e^{-S} \mathcal{N}(A), \quad (2.2)$$

where the sum runs over an ensemble \mathcal{S} of hyper-cubic surfaces with spherical topology. In the large volume limit, the number $\mathcal{N}(A)$ of surfaces with a given area A is expected to grow like

$$\mathcal{N}(A) \approx e^{\mu_c A} A^{\gamma-3}, \quad (2.3)$$

where γ is the entropy exponent. Let us for the moment consider the action with only one term:

$$S(\mu) = \mu A. \quad (2.4)$$

The partition function (2.2) is well defined only if the coupling μ is larger than the critical value μ_c . The continuum limit is obtained by taking the lattice spacing a to zero and at the same time $\mu \rightarrow \mu_c^+$.

There are three possible ways to embed two neighbor plaquettes p_1, p_2 in a hyper-cubic lattice Z^D . The external angle Θ_l , which we assign to link l , can therefore take three possible values:

- 0: p_1 and p_2 occupy two neighboring squares in the same coordinate plane,
- $\frac{\pi}{2}$: p_1 and p_2 occupy two neighbor squares in different coordinate planes,
- π : p_1 and p_2 occupy the same square. We call such a configuration self-bending.

The model defined so far describes what we called the unconstrained model. The constrained model considers the ensemble of hyper-cubic surfaces

$$\mathcal{S}' = \{S \in \mathcal{S} | S \text{ does not contain self bendings}\}. \quad (2.5)$$

This restriction can be formulated by introducing a potential

$$S_{ext}^{(1)}[E](\epsilon) = \epsilon \sum_{l \in E} \delta_{\pi, \Theta_l} \quad (2.6)$$

to the action with an infinite coupling ϵ . The angle Θ_l is the angle of two plaquettes, which have the edge l in common, measured in the embedding space. Therefore this term couples to the external curvature of the surface.

It seems a bit artificial that this potential only contains contributions from links l with $\Theta_l = \pi$. We therefore also use the potential

$$S_{ext}^{(2)}[E](\epsilon) = \frac{\epsilon}{2} \sum_{l \in E} (1 - \cos \Theta_l) = \epsilon \sum_{l \in E} \left(\delta_{\pi, \Theta_l} + \frac{1}{2} \delta_{\pi/2, \Theta_l} \right). \quad (2.7)$$

In summary: The action of our model is

$$S[E](\mu, \epsilon) = \mu A + S_{ext}^{(i)}[E], \quad i = 0 \dots 2 \quad (2.8)$$

where

$$S_{ext}^{(0)}(\epsilon) = 0 \quad (2.9)$$

formally denotes the action without a curvature term. The canonical partition function is

$$Z(A, \epsilon) = \sum_{E \in \mathcal{S}_A} e^{-S[E](A, \epsilon)}, \quad (2.10)$$

where the action S contains one of the external curvature terms discussed above. The sum runs over hyper-cubic- surfaces with fixed area A .

2.3 Universality

In this section answer the question of whether the constrained hyper-cubic random surface model has a critical behavior different from the unrestricted model as indicated by earlier numerical results [26] in four embedding dimensions. With the algorithms and the improved computer hardware available today we can simulate systems up to two orders of magnitude larger than those used in earlier works.

The model is defined by the partition function (2.2) where the summation runs over the constrained ensemble (2.5). The action (2.8, $i = 0$) contains no external curvature term. We measure the universal entropy exponent γ defined in (2.3), which is a good indicator for different phases of the model. For branched polymers it takes the value $\gamma = \frac{1}{2}$. A different value indicates a different geometry. This will become clearer in section 2.3.2 where we use a geometrical decomposition to measure the exponent γ .

2.3.1 Old method

As the first step we want to make sure that our program, which uses an algorithm different from the one used in the earlier works, gives the same answers if one uses a similar numerical setup. We simulate the grand canonical ensemble to extract the distribution $N_\mu(A)$ of surface areas measured with coupling μ . Taking into account the Boltzmann factor one can fit $N_\mu(A)$ to the theoretical distribution $\mathcal{N}(A)$ eq. (2.3). Besides an uninteresting normalization constant one gets an estimate for γ and $t = \mu_c - \mu$. However, one has to fine-tune μ very precisely so that $t = 0$, because for large (tA) the distribution is dominated by the leading exponential factor and therefore the sub-leading behavior is difficult to observe in this case. We have used this method anyhow for small surfaces and got a value for γ which is compatible with the results presented below.

In [26] a clever way to avoid this problem is used. The unknown parameter μ_c can be absorbed into a constant if one divides two histograms $N(A_1), N(A_2)$ with $\delta = A_1 - A_2$ kept constant :

$$\frac{N^{\mu_1}(A_1)}{N^{\mu_2}(A_2)} = \frac{e^{(\mu_c - \mu_1)A_1} A_1^{\gamma-3}}{e^{(\mu_c - \mu_2)A_2} A_2^{\gamma-3}} = c_{\mu_1}^{\mu_2} e^{(\mu_2 - \mu_1)A_1} \left(\frac{A_1}{A_2}\right)^{\gamma-3}. \quad (2.11)$$

In this case the factor

$$c_{\mu_1}^{\mu_2} = e^{(\mu_c - \mu_2)\delta} \quad (2.12)$$

is just a constant.

In the numerical simulations we use our Monte Carlo program to generate the distributions $N_\mu(A)$ for $\mu < \mu_c$. We prevent the surface from growing to infinity by introducing an upper bound A_{max} for the area. This does not spoil the detailed balance condition but ergodicity may in principle be affected for surfaces not much smaller than A_{max} . In the verification of the algorithm (section 2.5.1) we, however, did *not* observe any effect on the distribution of surfaces induced by the upper bound. Following [26] we have anyhow discarded the data for surfaces of size $[A_{max} - 20, A_{max}]$ when analyzing the data. We have measured $N_\mu(A)$ with two different A_{max} and for different couplings. In table 2.1 we summarize the number

	$A_{max} = 300$	$A_{max} = 5000$
$\mu = 1.60$		3×10^{10}
$\mu = 1.65$	1×10^{10}	3×10^{10}
$\mu = 1.70$	2×10^{10}	3×10^{10}
$\mu = 1.75$	1×10^{10}	

Table 2.1: Monte Carlo statistics in iterations collected for parameters A_{\max} and μ

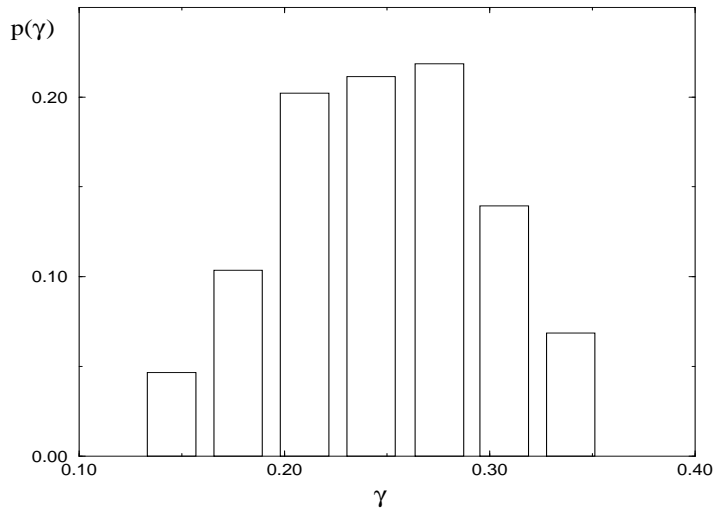


Figure 2.2: The distribution of γ values

of iterations collected for six different parameters A_{max} and μ . After dividing each dataset into three parts there are $9 \times 9 = 81$ ways to combine data for $A_{max} = 5000$ in formula (2.11) with data for $A_{max} = 300$. We have extracted γ for the 81 combinations. In figure 2.2 we show the distribution of γ values obtained with this procedure. Taking the average we get $\gamma = 0.26(2)$. This is in agreement with the result $\gamma = 0.24(3)$ in [26]. We have repeated the procedure for the model which allows for self-bending surfaces and found $\gamma = 0.44(3)$ which is in reasonable agreement with the expected result $\gamma = \frac{1}{2}$ [25].

2.3.2 The Baby universe method

The baby universe method [31] has become a standard tool for measuring the entropy exponent γ in numerical simulations of random surfaces. It is very convenient because it does not require fine tuning of parameters and allows the use of large systems in the simulation. In this section we present the numerical results

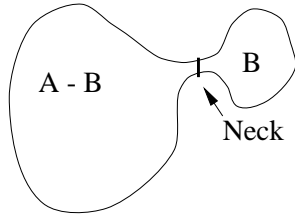


Figure 2.3: A baby surface

obtained with this method for hyper-cubic random surfaces with up to 80000 plaquettes. A baby-universe is a part of a surface S with the topology of a disc. It is connected with the rest of S in such a way that the disc-perimeter l is much smaller than the disc area B : $l^2 \ll B$. In figure 2.3.2 this is depicted graphically: a baby universe is a part of S connected to the rest of S by a bottle-neck. If one looks at this neck from far enough away one sees it as a point at which two surfaces are joined, one with area B , the other with area $A - B$, where A is the area of the whole surface S .

One can approximate the baby universe distribution [32] by :

$$N_A(B) \sim \mathcal{N}_l(B)\mathcal{N}_l(A - B) \quad (2.13)$$

where $\mathcal{N}_l(A)$ is the number of discs with loop l and area A . This number can be expressed by the number of spherical surfaces $\mathcal{N}(A)$ eq. (2.3). Consider for example the disc with area A and a unit-square as the boundary. Such a disc can be created by removing one plaquette from a spherical surface with area $A + 1$. Taking into account the factor $(A + 1)$ which counts the number of plaquettes that can be removed from the sphere one gets

$$\mathcal{N}_l(A) = (A + 1)\mathcal{N}(A + 1). \quad (2.14)$$

This formula is approximately true also for different boundary shapes. Substituting this expression and (2.3) in (2.13) gives

$$N_A(B) \sim c(A)(B(A - B))^{\gamma-2}(1 + \text{corr.}) \quad (2.15)$$

for the distribution of baby surfaces with area B on a surface with total area A . The leading exponential contribution $c(A) = c \exp(\mu_c(B + \{A - B\}))$ depends only on the area A of the whole surface and not on B .

This is very convenient in numerical simulations where one can use (2.15) to measure the exponent γ , which is part of a volume correction term in the canonical (fixed area) ensemble. This means that one does not need to fine-tune μ to μ_c . However, for technical reasons, we still have to tune with comparatively low precision the coupling μ to its pseudo-critical value μ_{pc} . Our algorithm is inherently grand canonical since ergodicity requires volume fluctuations. We extract the information for the canonical ensemble with $A = A_0$ from the simulated grand canonical ensemble by measuring only if $A = A_0$. Inefficient large volume fluctuations about A_0 are suppressed by a potential

$$U(A) = \frac{\delta}{2}(A - A_0)^2 \quad (2.16)$$

which we add to the action (2.8) with an appropriate choice of δ . We used $\delta = 0.002$ in the simulations. For the simulation the coupling μ has to be tuned so that $\langle A \rangle \approx A_0$. The Gaussian form of the grand-canonical ensemble allows us to estimate $\mu - \mu_{pc}$ by measuring $\langle A \rangle$, i.e.

$$\mu - \mu_{pc}(A_0) \approx \delta(\langle A \rangle - A_0). \quad (2.17)$$

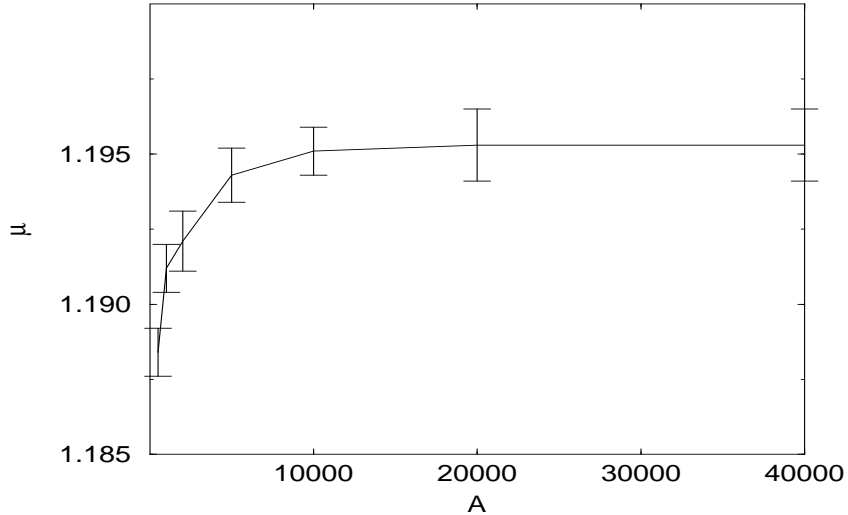


Figure 2.4: Pseudo critical coupling $\mu_{pc}(A)$

We use this formula to improve, recursively, the estimate for μ in the simulations. In figure 2.4 we show the pseudo-critical coupling obtained with this procedure.

We choose the coordinates

$$\begin{aligned} y &= \ln [(B(A - B))^2 N_A(B)] \\ x &= \ln [B(A - B)] \end{aligned} \quad (2.18)$$

to analyze the measured baby universe distribution $N_A(B)$. In these coordinates the exponent γ can be extracted from the numerical data with a linear fit to the equation $y = \gamma x + b$. In figure 2.5 we show a typical baby universe distribution using the coordinates (2.18). The total surface area is $A = 20000$. For small values of B we see clear evidence of finite size effects; the data-points do not lie on a straight line. On the other hand for large values of B one can see strong statistical noise which comes from the low frequency of large baby universes. For example, for $A = 10000$ the probability of finding a baby universes of area $B = 4999$ is 7×10^{-4} . When estimating the value of γ one has to deal with the finite size effects. In our analysis we discard data for small baby universes. To decide, which part should be kept, we look at the behavior of $\gamma_{eff}(B)$ obtained from the fit to the data for baby surfaces larger than B as a function of B . As one can see in figure (2.6), where we show as an example $\gamma_{eff}(B)$ measured for $A = 20000$, that $\gamma_{eff}(B)$ grows to a plateau value. We use this value to estimate γ_{eff} .

We analyzed the baby universe distribution for different canonical volumes. In figure (2.7) we show γ_{eff} as a function of the canonical volume A . For comparison we also performed simulations for the unrestricted ensemble. As discussed above, for this case one can show analytically that $\gamma = \frac{1}{2}$. For the constrained model without self-bendings (lower curve) one observes stronger finite size effects. The asymptotic value of γ_{eff} , however, is the same. We conclude that the constrained

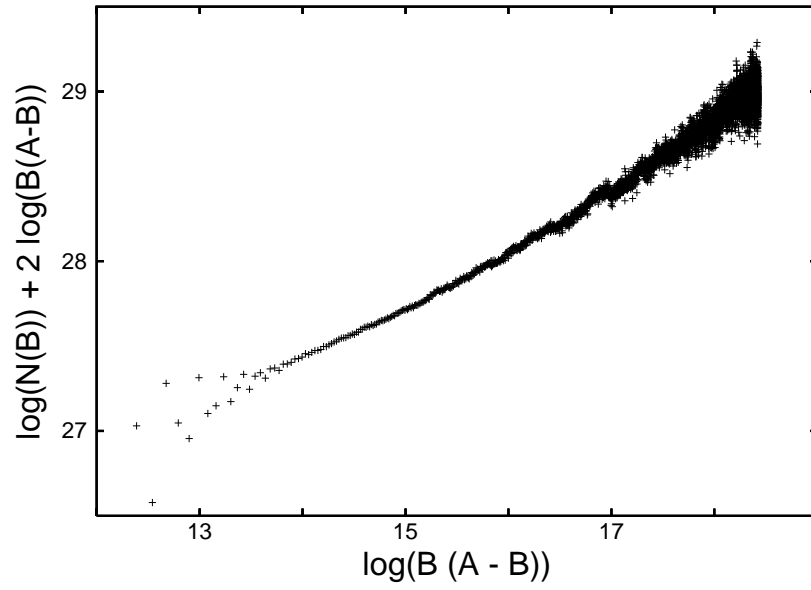


Figure 2.5: The distribution of baby-surface areas for $A = 20000$

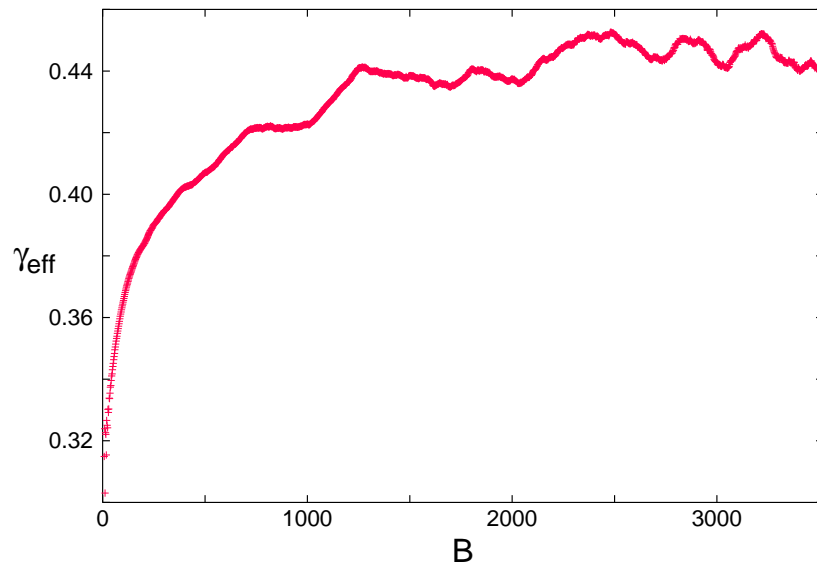


Figure 2.6: The effective γ_{eff} as a function of the lower cut-off B for $A = 20000$.

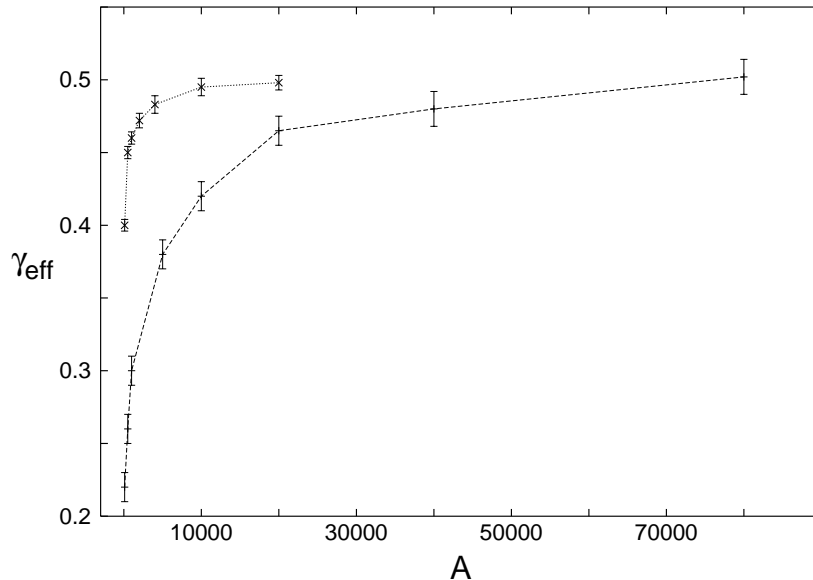


Figure 2.7: The effective entropy exponent γ_{eff} as a function of the canonical volume A for ensembles including (upper curve) or excluding (lower curve) self-bending, respectively.

hyper-cubic random surface model possesses the same critical behavior as the unconstrained model. This means that the model is universal in the sense that the details of the discretization are unimportant. However the result $\gamma = \frac{1}{2}$ contradicts the results obtained with the method used in [26], presented in the previous section. The reason for this contradiction is easy to understand if one looks at figure 2.7. In the last section surfaces with an area $200 < A < 280$ were used to extract an estimate for γ . From figure 2.7 one sees that for surfaces of this size the effective $\gamma_{eff} \approx 0.25$; on such small surfaces the finite size effects are still dominating.

2.3.3 Discussion

We have measured the value of the string susceptibility exponent γ for hyper-cubic surfaces embedded in a 4 dimensional target space for an ensemble of spherical surfaces with and without self-bendings. In both cases we find numerically, for large enough surfaces, $\gamma \approx 1/2$, which is compatible with a branched polymer behavior. The local constraint first discussed in [26] is not sufficient to change the critical behavior of the model. However, in the next section we will show that a generalized external-curvature term can change this behavior.

It is intriguing to note that the discretized model of Nambu-Goto strings suffers from the same pathological behavior as that of Polyakov string theory. It collapses down to a branched polymer, i.e. essentially a one-dimensional object. This result suggests that both models have the same universal behavior. Unfortunately the Nambu-Goto string is not defined in $D < 2$, so it is not possible to compare the discretized string models in $D < 1$ where one finds non-trivial behavior for the Polyakov string.

2.4 Hyper-cubic random surfaces with extrinsic curvature

2.4.1 Introduction

The branched polymer behavior of the constrained hyper-cubic random surface does not rule out the possibility that one finds non-trivial behavior for the model with the generalized extrinsic curvature action (2.7). With infinite coupling ϵ the generic surface is, up to finite size effects, flat. For finite couplings one may hope to find a transition from the branched polymer to a flat phase.

However it was shown in [33] for the model with extrinsic curvature that "the critical exponents take their mean field value if the susceptibility of the model and a coarse grained version of it both diverge". In other words under the assumptions

$$\gamma > 0 \quad \text{and} \quad \bar{\gamma} > 0. \quad (2.19)$$

the model is always in the branched polymer phase. This result was obtained with a renormalization group argument where the branched polymer was decomposed into "blobs", components which can not be cut into two parts along a loop of length two. The exponent $\bar{\gamma}$ is the entropy exponent for these blobs. The equivalence of (2.19) with the statement given above can be seen from the expected behavior of the susceptibility

$$\chi(\mu) \approx (\mu - \mu_c)^{-\gamma}, \quad (2.20)$$

which diverges for $\mu \rightarrow \mu_c$ only if $\gamma > 0$.

A key step in the derivation of this result in [33] is the formula

$$\chi(\mu) = \frac{\bar{\chi}(\bar{\mu})}{1 - \bar{\chi}(\bar{\mu})} \quad (2.21)$$

which relates the susceptibility $\chi(\mu)$ of the original model to the susceptibility $\bar{\chi}(\bar{\mu})$ of the decomposed blobs with renormalized coupling $\bar{\mu}$. Obviously $\bar{\chi} = 1$ if the susceptibility χ diverges. Under the assumptions stated above, i.e. $\bar{\gamma} > 0$ for the blobs one concludes that they are not critical $\bar{\mu} > \bar{\mu}_c$ and $\bar{\chi}$ is analytic at this point. With a Taylor expansion one gets the self consistency relation $\gamma = 1 - \bar{\gamma}$ which is solved by $\gamma = \frac{1}{2}$, the generic value for branched polymers.

However, Durhuus emphasized in [30] that the condition $\bar{\chi} = 1$ alone does not imply that the blobs are non-critical. If $\bar{\gamma} < 0$ the susceptibility $\bar{\chi}$ does not diverge and $\bar{\chi} = 1$ can be satisfied *at* the critical point $\bar{\mu} = \bar{\mu}_c$ of the coarse grained system. At such a point the entropy is still dominated by the branching of the surface but the branches themselves are critical, which in effect changes the exponent γ for the whole system. If one assumes that $\bar{\gamma}$ takes the KPZ-values (1.25) one can derive from (2.21) the series (2.1).

The derivation of that formula is rather formal. It does not provide a description how to construct a system which has this property. We want to check numerically if the hyper-cubic random surface model exhibits non trivial behavior at an eventual crumpling transition. In other words we check if the assumptions (2.19) are fulfilled in the whole range of couplings ϵ . Non-trivial behavior can be expected only if these assumptions are not satisfied, which we expect if $\epsilon = \epsilon_c$ is at a critical point.

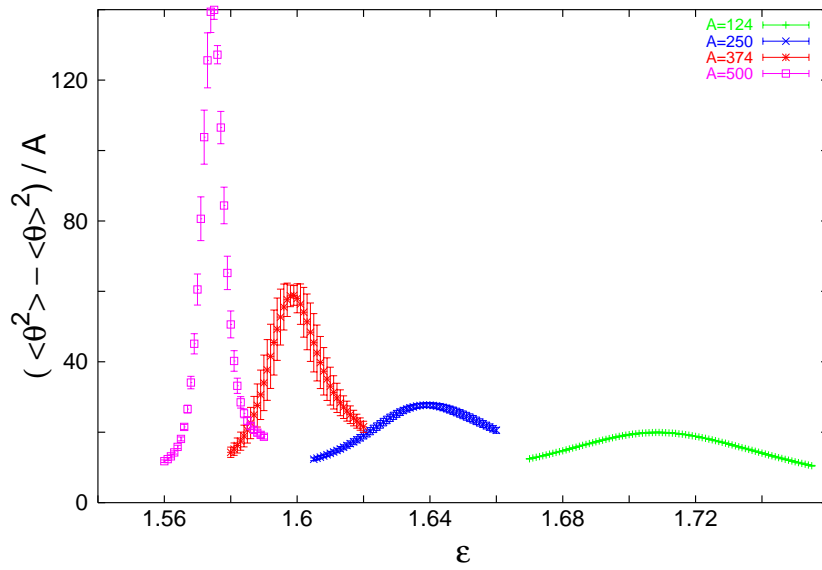


Figure 2.8: The susceptibility χ_{ext} in $D = 3$ dimensions

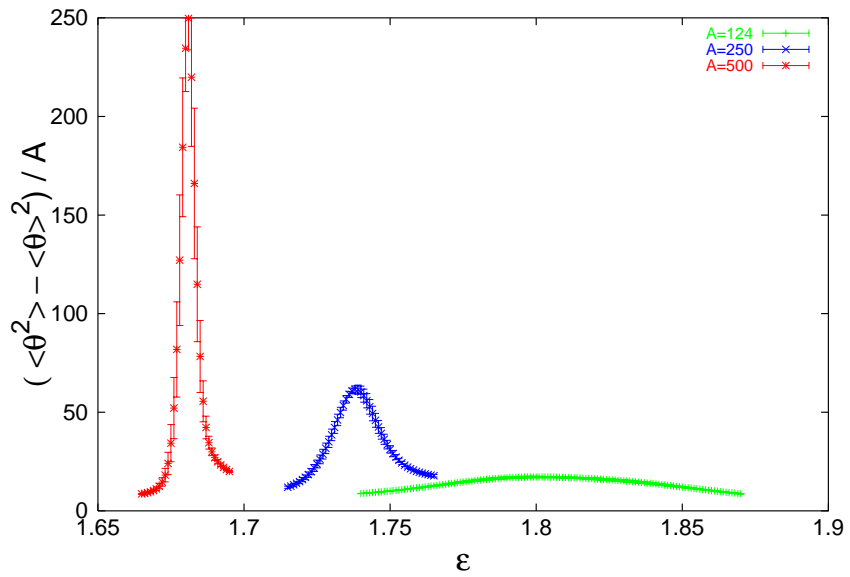


Figure 2.9: The susceptibility χ_{ext} in $D = 4$ dimensions

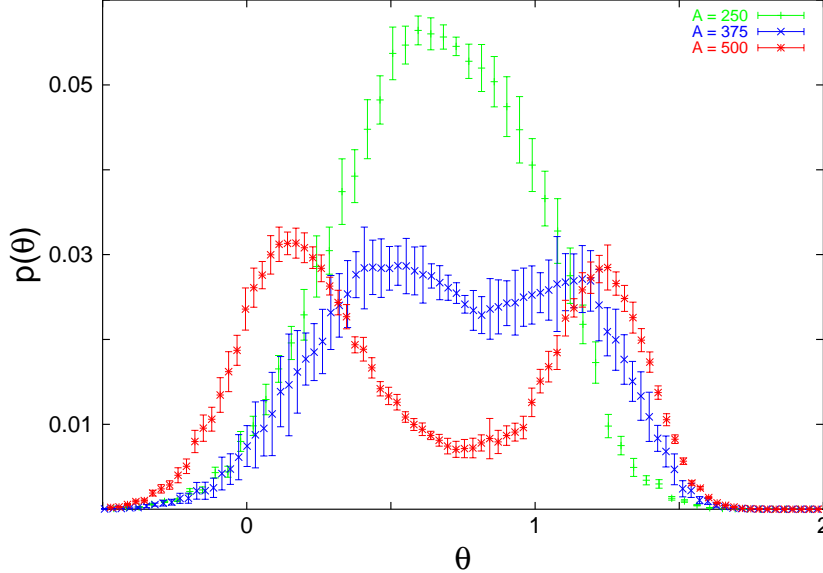


Figure 2.10: The distribution of the average external curvature $\bar{\Theta}$ in $D = 3$ dimensions obtained with re-weighting. The non zero probability for unphysical negative values $\bar{\Theta} < 0$ is an artifact of the extrapolation to this region in the re-weighting process.

2.4.2 Numerical results

The simulations are done in the same quasi-canonical way already discussed for the constrained model eq. (2.16). To localize possible transitions we measure the energy fluctuation of the external curvature field

$$\chi_{ext} = \frac{1}{A} \frac{\partial^2}{\partial^2 \epsilon} \log Z(A, \epsilon) = \frac{\langle \Theta^2 \rangle - \langle \Theta \rangle^2}{A} \quad (2.22)$$

and search for a peak in this observable. The average external curvature is proportional to the first derivative of the free energy :

$$\langle \Theta \rangle = \frac{\pi}{2A} \frac{\partial}{\partial \epsilon} \log Z(A, \epsilon) = \frac{1}{2A} \sum_S \sum_l \Theta_l e^{-S[E]}. \quad (2.23)$$

We simulated in both three and four embedding dimensions and scanned the coupling range $0 \leq \epsilon \leq 3$ for peaks of χ_{ext} . In both cases we found a single peak. We used re-weighting methods [34] to extract the shape of the peaks shown in figures 2.8 and 2.9 from four independent measurements at $\epsilon \approx \epsilon_{pc}$ per volume.

The peaks grow quickly, in fact a bit faster than linearly, with the volume. This indicates a first order phase transition, which is confirmed by a look at the distribution of external curvature $\bar{\Theta}$, where the bar indicates the average taken over a given lattice. In figure 2.10 we show this distribution for $D = 3$ and the coupling $\epsilon \approx \epsilon_{pc}$ close to the pseudo-critical coupling. One observes a clear signal of a first order phase transition, namely two maxima separated by a minimum which becomes deeper as the size of the surfaces is increased. This clearly indicates two

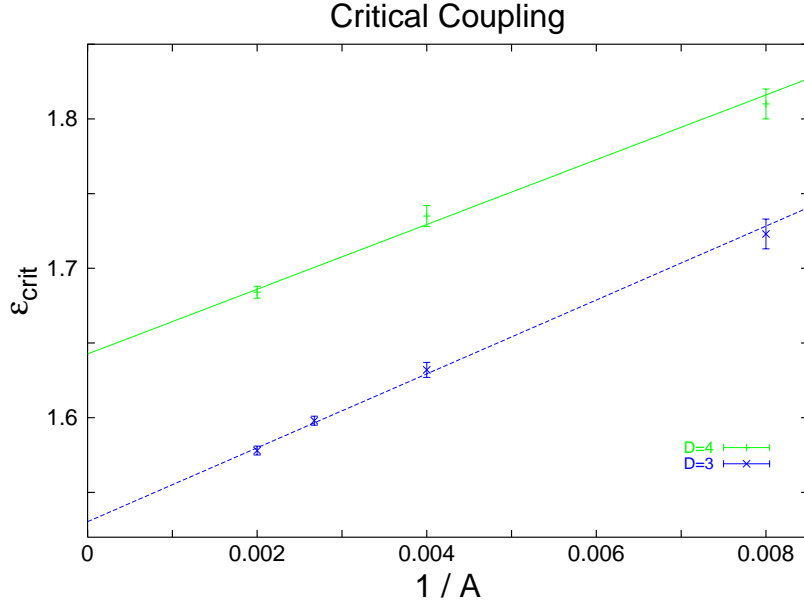


Figure 2.11: The pseudo-critical coupling $\epsilon_{crit}(1/A)$.

separate phases. In one phase the average external curvature is close to zero, the typical surface is flat.

To estimate the critical coupling we use that for a first order phase transition one can expect

$$\epsilon_{pc}(A) = \epsilon_c + \frac{c}{A} + O\left(\frac{1}{A^2}\right) \quad (2.24)$$

for the scaling of the pseudo-critical couplings ϵ_{pc} . In figure 2.11 we show the numerical estimates for ϵ_{pc} . Note that the pseudo critical coupling decreases with the volume which indicates that ϵ_c is finite in the thermodynamical limit. With a linear fit to equation (2.24) we find for the critical coupling

$$\begin{aligned} D = 3 \quad \epsilon_c &= 1.530(3) \\ D = 4 \quad \epsilon_c &= 1.643(4) \end{aligned}$$

To demonstrate the change in the geometrical behavior we consider the radius of gyration

$$G^2(A, \epsilon) = \left\langle \frac{1}{A} \sum_{p_{x,y}} (S_\mu(p_{x,y}) - S_\mu(p_0))^2 \right\rangle, \quad (2.25)$$

which is the average squared distance of the plaquettes to some reference plaquette p_0 . The S_μ are the coordinates of the plquette in the embedding space. In the numerical simulations we do a stochastic average over the p_0 by choosing about 10 % of the plaquettes at random as p_0 per measurement. One can use the radius of gyration to define the external Hausdorff dimension d_h

$$G^2(A, \epsilon) \approx A^{2/d_h}. \quad (2.26)$$

In a sense the Hausdorff dimension is the largest possible dimension for the embedding space which can still be completely filled by the surface. One has for example

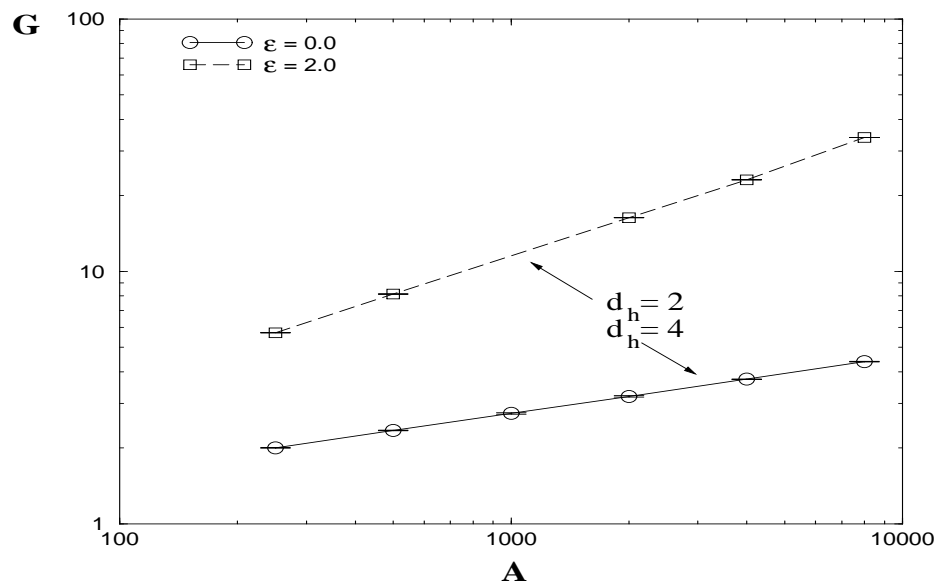


Figure 2.12: The scaling of the radius of gyration.

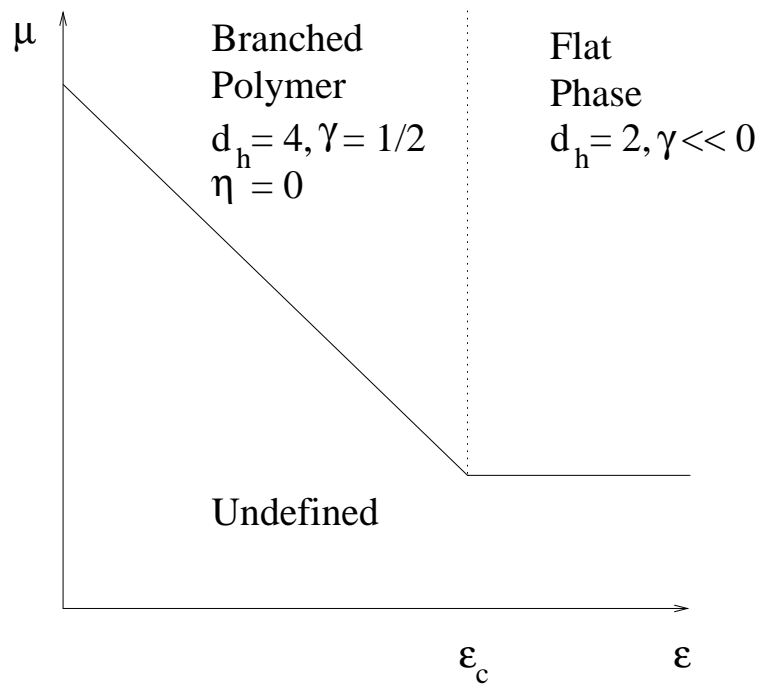


Figure 2.13: The phase diagram for the Hyper-cubic random surface model with extrinsic curvature. One finds qualitatively the same behavior in $D = 3$ and $D = 4$ embedding dimensions.

$G^2 \propto A$ for a flat surface and therefore $d_h = 2$. In figure 2.12 we show $G(A, \epsilon)$ measured in the branched polymer phase, at $\epsilon = 0$, and in the strong coupling phase, at $\epsilon = 2.0$. With a fit to (2.26) we extract the Hausdorff dimension in the two phases:

$$\begin{aligned} \epsilon = 0. & \quad d_h = 4.07(3) \\ \epsilon = 2. & \quad d_h = 2.00(3). \end{aligned}$$

The value found for $\epsilon = 0$ is two standard deviations away from the expected result [26] but this should presumably be attributed to finite size effects.

The results are summarized in the phase diagram figure 2.13. The model is defined only for $\mu > \mu_c(\epsilon)$ which defines the critical line depicted by the solid line in the phase diagram. Above this line we find two phases. For $\epsilon < \epsilon_{crit}$ the system is in the branched polymer phase with $d_h \approx 4$. If we assume hyper scaling

$$\nu = d_H^{-1}, \quad \gamma = \nu(2 - \eta) \tag{2.27}$$

the anomalous scaling dimension is $\eta = 0$ as expected for a branched polymer. The strong coupling phase is flat with $d_h = 2$. In this phase basically no baby universes are present. For example, on a surface of size $A = 500$ we found at $\epsilon = 2$ on average only 0.06 baby universes of size $B = 5$. The largest one found in this phase is of size 33 and appeared only once in 200000 measurements. For comparison in the branched polymer phase at $\epsilon = 0$ we found in average 10.6 baby universes of size 5 on the surface, the probability for the largest possible one with $B = 249$ is about 0.02. Therefore one can not use the baby universe distribution to measure γ in the flat phase. However the fact that there effectively are no baby surfaces means that γ is large negative. Therefore the existence of this phase is not in contradiction with [33] because the assumptions (2.19) are not met.

We hoped to find $\bar{\gamma} < 0$ for the branches at the critical point. Instead we found γ for the whole system large negative in the strong coupling phase. At the transition point the exponent γ is not well defined because the transition is first order with different values for γ in both phases. The close to horizontal critical line in the phase diagram fig. 2.13 for the flat phase reflects the fact that the curvature field is almost frozen at $\langle \Theta \rangle = 0$. A increase of the coupling ϵ has no further effect on the geometry and therefore also no effect on the entropy $\log(\mu_c)$ of the surface.

2.4.3 Discussion

We have investigated the phase diagram of hyper-cubic random surfaces with an extrinsic curvature term in the action. We find two phases. The weak coupling phase is dominated by branched polymer structures with $\gamma = 1/2$. The strong coupling phase is flat. The transition between the two phases is first order. We show that the existence of the flat phase is not in contradiction with [33].

In three dimensions one can interpret the hyper-cubic surfaces also as membranes. The internal geometry in this model is dynamic, therefore the surfaces are called fluid membranes. However, they are not self-avoiding. Self-intersection is, differently from typical membranes, allowed. The first order phase transition, which we reported in this work, is therefore an example for a phase transition of fluid membranes at finite coupling. For fluid membranes described by dynamical

triangulations with an extrinsic curvature term the existence of a phase-transition flat phase is disputed. In [36] numerical evidence in favor for a second order phase transition was reported. The authors of [37, 38] can not exclude that it is a cross-over rather than a phase transition. For fluid membranes with an external curvature term in the action a renormalization group analysis [39, 40, 41, 42] indicates that there should be no stable flat phase at a finite coupling to the external curvature.

We cannot take a continuum limit at the transition point because the transition is of first order. It is possible that the transition might become softer, and continuous, if one introduces self-avoidance into the model. This is for example the case for a model of Ising-spins with a gonihedric action [43]. This model is dual to a surface model with extrinsic curvature. It does, however, not define the internal connectivity of the surface when more than two plaquettes meet at an external link. Numerically a first order phase transition was found [44], but with a weak self-avoidance imposed evidence for a second order phase transition was found [45].

2.5 The Algorithm

The algorithm used in the simulations in this chapter is a Monte Carlo algorithms which was discussed in section (1.7). In this section we want to describe the transformations (1.54) and the weight (1.59) specific to our new algorithm for the hyper-cubic random surface model.

The transformations are based on a set of local moves depicted in figure 2.14. A prescription for all four pairs of moves is the following: choose p connected plaquettes (drawn shaded in the figures) on the surface such that they form a part of a sphere (a cube) and replace them by the rest of the sphere, the transparent $q = 6 - p$ plaquettes in the figures. We denote by M_{pq} a move where p is the number of plaquettes being removed and q the number of plaquettes inserted into the surface. Consider for example the move M_{15} which removes a single plaquette from the surface and fills the hole with a "house" of five plaquettes. In the reverse move the role of the shaded and transparent plaquettes is interchanged. For example deformation M_{51} replaces a house with a single plaquette. Deformations M_{33a} and M_{33b} are self dual, i.e. if one deforms the "same" location twice with one of these moves the surface is unchanged.

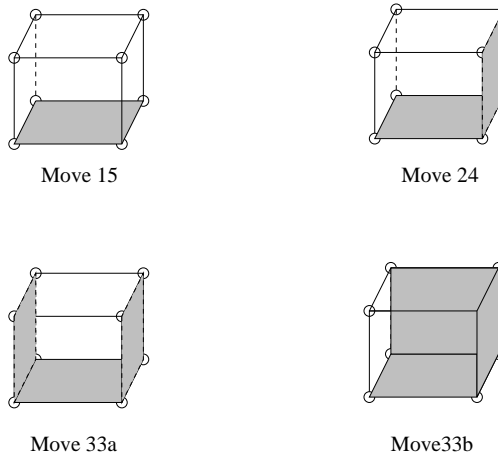


Figure 2.14: An ergodic set of deformations

The moves M_{pq} shown in figure 2.14 are known to be ergodic [35]. The additional moves which we discuss now are therefore not necessary for ergodicity. However, they turn out to improve the mobility of the algorithm. The move M_{02} shown in figure 2.15 cuts open a link and inserts a spike. A spike are two plaquettes glued together along three edges. The move M_{00} is a non-local deformation in terms of the internal geometry but is local in the embedding space. It cuts open two different (internal) links, which occupy the same link in the embedding, and it cross-connects the plaquettes. This can probably better be understood in the dual representation. In the dual representation a plaquette is replaced by a vertex, links are replaced by propagators and a vertex is dual to a closed propagator. However not all closed propagator loops are dual to a vertex. One can easily convince oneself that only those loops which turn to the right (left) at each vertex of the loop are dual to a

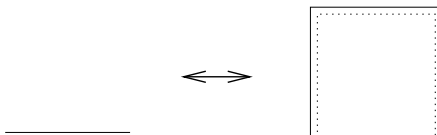


Figure 2.15: Spike insertion / deletion

vertex on the hyper-cubic lattice. The move M_{00} cuts open two such propagator loops and glues pairwise together the free ends of the two loops, provided this is allowed geometrically. In figure 2.16 we show an example of such a transformation. The diagram on the left is dual to two spikes glued together along their open links. Under the geometric constraint that the two spikes occupy the same unit-square in the embedding one can cut open one edge, say the edge to the right from the common one, and glue the now free edges pairwise together. After doing this one ends up with a "bag in a bag" where a "bag" are two surfaces glued along two edges with a common corner. Note that the surfaces may not be glued together on opposite edges because the latter configuration has a different topology, that of a torus.

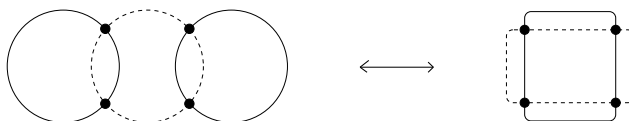


Figure 2.16: An example of move M_{00} in the dual representation

A transformation is done in the following steps:

1. Choose a location A for the deformation.
2. Choose a move M_{pq} from the set of deformations
3. Choose a direction or orientation d . For example in move M_{15} one can choose in which of the $2(d-2)$ possible directions the house should be built.
4. Check if the move violates any geometrical constraints. If not, subject it to a Metropolis test.
5. Apply the local deformation M_{pq} at A in direction d .

The Monte Carlo weights π_{pq} for deforming the surface at a specific place by move M_{pq} can be derived from the detailed balance condition (1.57)

$$\pi_{pq} \frac{1}{A} \frac{1}{n_m} \frac{1}{n_d} e^{-S[\mathcal{A}]} = \pi_{qp} \frac{1}{A+p-q} \frac{1}{n_m} \frac{1}{n'_d} e^{-S[\mathcal{A}']}. \quad (2.28)$$

The factor $p = \frac{1}{A}$ is the probability of choosing certain plaquette from the A plaquettes which form the surface before the move. The grand canonical moves discussed above change the size of the surface to $A+q-p$. The probability of choosing the correct location for the inverse transformation is $\frac{1}{A+p-q}$, which is different from p .

Therefore the probabilities π_{pq} contain an area dependent pre-factor to balance the grand canonical fluctuations in the transformation probabilities. The next term $1/n_m$, the number of possible moves, however, drops out because in the second step of the transformation the probability to choose a certain transformation is the same for a move and its inverse. The next factor takes into account the freedom one has in choosing a direction. For example in move M_{15} one can choose from $2(D - 2)$ directions orthogonal to the chosen plaquette. In the inverse transformation M_{51} one has no freedom after choosing the roof of a house to be removed. The last factor is the Boltzmann distribution which we want to generate. Note that the action contains contributions from the external curvature. The weights coming from the field can be used directly because the curvature field has no degrees of freedom of its own. In the following table we list the transition probabilities for the different moves. The numbers n_a, n_b give the number of allowed deformations of the type M_{00} at the specific site of the lattice.

M_{15}/M_{51}	$\frac{\pi_{15}}{\pi_{51}} = 2 \frac{A}{A+4} (d - 2) \exp(\Delta S)$
M_{24}/M_{42}	$\frac{\pi_{24}}{\pi_{42}} = \frac{A}{A+2} \exp(\Delta S)$
M_{33a}/M_{33b}	$\pi_{33a} = \pi_{33b} = \exp(\Delta S)$
M_{02}/M_{20}	$\frac{\pi_{02}}{\pi_{20}} = 8 \frac{A}{A+2} (d - 1) \exp(\Delta S)$
M_{00}	$\pi_{00} = n_a/n_b$

2.5.1 Verification

To check the validity of the algorithm and its implementation we simulated very small surfaces E and compare the distribution of surfaces with a theoretical distribution which we have calculated explicitly for the smaller surfaces. To avoid too many technicalities we present here in detail only the verification for the model without the extrinsic curvature term in the action. In table (2.2) we list the smallest diagrams. The number \mathcal{N} is the number of possible embeddings in the embedding space compatible with the internal geometry of the surface. The symmetry factor σ are also given. Below we will show that the weight of a graph is \mathcal{N}/σ . We list the weight in the columns $d = 2, d = 3$ for two and three dimensions. In the last column the weight measured numerically with our algorithm in $d = 3$ dimensions is given. They are in perfect agreement with the theoretical values.

In writing the partition function (2.2) we were a bit sloppy because we have silently dropped the symmetry factor $\sigma(E)$. The justification for doing so is the fact that the typical large surface considered so far is not symmetric and hence for almost all large surfaces $\sigma = 1$. The small surfaces we consider now however are quite symmetric with $\sigma > 1$ and hence the factor becomes important. The precise partition function is

$$\mathcal{Z}(\beta) = \sum_{E \in \mathcal{S}} \frac{1}{\sigma(E)} e^{-S[E]} = \sum_{\text{Diagrams}} e^{-S[E]} \frac{\mathcal{N}(E)}{\sigma(E)}. \quad (2.29)$$

In the rightmost expression we re-express the partition function as a sum over diagrams. The number $\mathcal{N}(E)$ counts the number of possible ways of embedding a surface dual to the diagram E in the D -dimensional space. This number is most

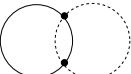
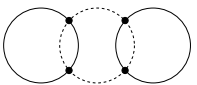
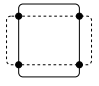
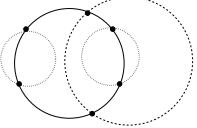
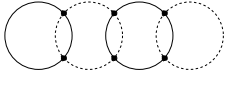
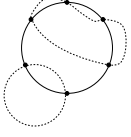
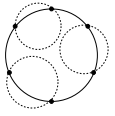
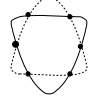
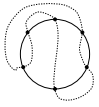
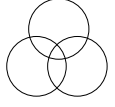
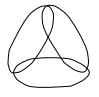
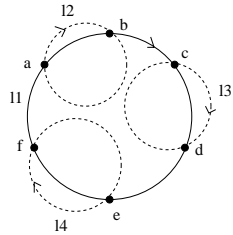
	Diagram	$\sigma(E)$	$\mathcal{N}(E)$	d=2	d=3	N
a		8	$4d(d-1)$	1	3	3.01(2)
b		4	$8d(d-1)^2$	4	24	23.98(4)
c		8	$4d(d-1)$	1	3	3.00(2)
d		4	$16d(d-1)^3$	8	96	95.97(8)
e		2	$16d(d-1)^3$	16	192	192.000
f		1	$8d(d-1)^2$	16	96	96.00(9)
g		6	$16d(d-1)^3$	5 1/3	64	63.99(6)
h		12	$4d(d-1)$	2/3	2	2.09(11)
i		4	$4d(d-1)$	2	6	5.97(8)
j		24	$8d(d-1)(d-2)$	0	2	1.98(10)
k		6	$8d(d-1)(d-2)$	0	8	8.03(6)

Table 2.2: Diagrams of size 2,4,6, the symmetry factor σ , the number of embeddings \mathcal{N} , the theoretical weight in $d = 2$ and $d = 3$ dimensions and the distribution N obtained numerically in $d = 3$. The numerical distribution is normalized such that diagram e has weight 192.



a	b	b	b	f	2	1
b	c	a	a	a	1	2
c	d	d	d	b	3	1
d	e	c	c	c	1	3
e	f	f	f	d	4	1
f	a	e	e	e	1	4

abcdef	1234	++++
cdefab	1342	++++
efabcd	1423	++++
dcbafe	1324	-+++
bafedc	1243	-+++
fedcba	1432	-+++

Table 2.3: The adjacency matrix (top right) for diagram g using the choice of labels given in the top left diagram. The lower table lists the six re-labelings which leave the diagram unmodified.

easily counted in the geometrical representation. In the following we describe how to calculate σ .

To depict the diagrams used to verify the algorithm we choose the dual representation in table 2.2. The hyper-cubic surface model is dual to a M^4 -theory [46]. The M are hermitian matrices. The graphs are therefore fat graphs discussed in context with the matrix model in section 1.5. For clarity, however, we show only the thin graphs, known from scalar ϕ^4 theories, although they do not contain a complete description of the geometry. For example a ϕ^4 graph does not allow to define the geometrical property of two propagators being 'opposite' to each other because without the indices carried on a fat graph the propagators interacting at a vertex can not always be distinguished. In all graphs shown in this section we use the convention to draw propagators which are dual to opposite links on the surface as opposite links emerging from a vertex. By propagator loops we denote closed propagator loops which go along opposite propagators only, i.e. which do not form a right angle at any vertex. Geometrically this is a walk on the surface with one internal coordinate kept constant.

The symmetry factor σ for the diagrams is a discrete remnant of the reparametrization group. When drawing a diagram one has a choice of how to label vertices and propagator loops. We consider oriented surfaces, therefore one has also a freedom in the choice of the orientation of the loops in the dual diagram. Note that all this involves only internal properties of the diagram, the embedding is unimportant for this. The symmetry factor σ counts the number of relabelings which lead to the same diagram. For not too large diagrams one can directly probe all possible

$$N! l! 2^l \tag{2.30}$$

relabelings for a diagram with N vertices and l propagator loops and count the

number of invariant relabelings. As an example consider diagram g . In table 2.3 the adjacency matrix for this diagram with the labels depicted in the left-hand figure is written down. One can easily convince oneself that the relabelings listed in table 2.3 leave the diagram unmodified. The first transformation is the identity transformation, number two has to be interpreted as follows: Rename vertex $a \rightarrow c, b \rightarrow d, \dots$, loops $1 \rightarrow 1, 2 \rightarrow 3, \dots$ and maintain the orientation for loops $1, 2, 3, 4(+ + +)$. We found six invariant transformations, the symmetry factor for this diagram therefore is $\sigma = 6$.

Chapter 3

Four dimensional simplicial quantum gravity

3.1 Introduction

Quantum gravity in four dimensions, as defined by the path integral (1.30) and the action (1.31), is very difficult to deal with. The standard tool perturbation theory does not work because the model is not renormalizable. This can be seen from the fact that the coupling constant G has a negative mass dimension. Higher order loop corrections will therefore always generate more counter terms.

One possible interpretation of the breakdown of perturbation theory is that general relativity is not applicable at the Planck scale and is just a low energy effective theory of some unknown underlying theory. QCD, which is a renormalizable theory, provides us with an example of this: the effective low energy theory for the pion is non renormalizable. One possible candidate for the underlying theory of quantum gravity is string theory.

On the other hand, a somewhat more conservative interpretation is that the divergences in the perturbative expansion do not necessarily mean that general relativity does not work at the Planck scale. It may be that they appear just because of the naive way we do perturbation theory, we perturb around the wrong ground state. The theory may instead be well defined at some non-perturbative UV -fixed. Similarly to the nonlinear σ model, which is asymptotically UV free [47], the concept of asymptotic safety of four dimensional gravity was introduced [48]. It assumes the existence of a safe sub-space of the coupling space. For couplings on the safe surface the renormalization flow leads to a safe non-perturbative UV -fixed point. This conjecture is supported by the dimensional $2 + \epsilon$ expansion starting from two dimensional quantum gravity, where an UV -fixed point was found [49] for $\epsilon = 2$. The model considered in this chapter, four dimensional quantum gravity, may provide us with a candidate for the fixed point.

The structure of four dimensional manifolds is far less understood than in two dimensions. For example, there does not exist a topological classification of four-manifolds. In this situation the definition of the measure $\frac{\mathcal{D}[g]}{Vol(Diff)}$ is very difficult. One major conclusion of dynamical triangulations (see section 1.5) is the fact that

the sum over discrete triangulations, which replaces (1.33), defines the measure for the two dimensional model in a sensible way. This is a justification for *assuming* that the corresponding sum in the generalized four dimensional model, known as four dimensional simplicial quantum gravity, defines a sensible measure as well. The assumption implies that the reparametrization degrees of freedom are removed in the discrete model. In fact, diffeomorphism invariance is completely lost because one can not deform smoothly the discrete structure, which we describe in the next section. However, the basic symmetry group of general relativity is reparametrization invariance. One therefore has to check whether this invariance is restored in the continuum limit of the discrete model, if it exists.

Simplicial quantum gravity in four dimensions has been extensively studied by various groups. The main results are briefly summarized at the end of section 3.2. In the beginning, the results looked quite promising. In the recent years however it became clearer that the model as it stands has some problems. In numerical simulations it was found that the model has two phases. The dominating geometries in these phases are, however, not extended four dimensional geometries as one would expect. The weak coupling phase shows the behavior of branched polymers, essentially one dimensional highly branching thin tubes. The strong coupling phase is crumpled with a large connectivity. It has an infinite internal Hausdorff dimension. The transition between the two phases is first order [50, 51].

Based on calculations which assume that mainly the conformal deformations are important and ignore transverse excitations of the metric, it was suggested in [52] that the collapse to branched polymers can be prevented by coupling matter-fields to the model. This is opposite to what happens in two dimensions where additional matter drives the system into a branched polymer phase¹. In section 3.4 we investigate the phase diagram of the model with multiple vector fields and show that indeed the branched polymer phase disappears.

Another open question in four dimensional quantum gravity is what is the importance of topological excitations. It is not a priori clear, whether in the path-integral formulation of quantum gravity the sum over metrics should also run over topologies. It seems a bit artificial to fix the topology. Let us for the moment consider spherical topology. One may ask then why space-time can branch but is not allowed to join. Branches do not change the topology but if the branches re-join the manifold has a hole, i.e. it is not a sphere anymore. In two dimensions it can be shown that the naive sum over topologies diverges. In the double scaling limit, however, it is possible to define the model with the inclusion of all topological excitations. Using this two dimensional case as a guidance we have checked numerically whether in four dimensions a similar scaling is possible.

3.2 Simplicial quantum gravity

The dynamical triangulations model described in section 1.5 is an example how to discretize the space of metrics. In this two dimensional model the integral over equivalence classes of metrics is replaced by a sum over triangulations. Simplicial

¹See also section 2.1.

quantum gravity generalizes this discretization to three [53] and four [54, 55] dimensions. In what follows we use $D = 3, 4$. The integral over equivalence classes of D -dimensional metrics is replaced by a sum over D -dimensional simplicial manifolds. A D -dimensional simplicial manifold is a simplicial complex K with the additional constraint that the neighborhood of each vertex $p \in K$ is homeomorphic to a D -dimensional ball. A simplicial complex is built from d -simplices, where a d -simplex contains $d + 1$ vertices. A 0-simplex is a point, a 1-simplex a link, a 2-simplex a triangle and 3-simplex a tetrahedron and so on.

In one and two dimensions a simplicial manifold can be built by gluing together d -simplices along their $d - 1$ faces. Each complex constructed in this way satisfies the manifold condition. In higher dimensions the resulting complex may however violate the manifold condition, i.e. the neighborhood of a vertex is not homeomorphic to the D -ball. One can derive relations for the numbers N_i of i -simplices on the manifold which are known as Dehn-Sommerville relations [56]:

$$N_i = \sum_{k=i}^D (-1)^{k+D} \binom{k+1}{i+1} N_k. \quad (3.1)$$

These equations are not independent, they can, however, be used to eliminate the N_{2i+1} in even and N_{2i} in odd dimensions. One can use the discrete expression for the Gauss Bonnet theorem (1.32), the Euler relation

$$\sum_{i=0}^D (-1)^{i+d} N_i = \chi_d, \quad (3.2)$$

to eliminate one more N_i , the character χ_d is a topological invariant. This means that in $D = 3, 4$ only two of the N_i are independent.

So far we have defined a geometry but not a metric. A Riemannian metric is obtained by demanding that:

- The metric is flat inside a D -simplex
- The metric is continuous at the $D - 1$ dimensional faces of the d -simplex.
- The $(D - 1)$ dimensional faces of a D -simplex S are flat linear subspaces of S .

With this definition the metric inside a D -simplex S is determined by the length of the 1-simplices $s_i \in S$. As we will motivate below simplicial quantum gravity considers only manifolds with fixed edge lengths $l(s_i) = a$.

To define a path integral of the form (1.30) for simplicial manifolds we sum over all metrics, which can be represented by such manifolds. In the Regge approach (see for example [57]) one considers the metric space obtained by varying the edges length a_i on a simplicial manifold with *fixed* connectivity. It is however quite difficult to respect the geometrical constraints imposed on the a_i 's in the integration. Furthermore, a metric is not uniquely parameterized by the a_i 's. Therefore one has to deal with an unknown weight. Consider for example the triangulation T of a flat surface with equal edges length. Moving a vertex in the plane of the surface

obviously does not change the metric, although this degree of freedom is integrated over in Regge gravity. On the other hand metrics which are very different from the manifold T , are represented by singular simplices which contain extremely short or long edges length. It is therefore not obvious whether integration over the a_i really covers the whole space of metrics.

Simplicial quantum gravity tries to avoid the mentioned problems by summing over *dynamical* simplicial manifolds \mathcal{T} . In other words the dynamics of the model now lies in the connectivity of the simplicial manifold. The next step is to pick up a parameterization $a_i = a$. This introduces an UV cut-off into the model and removes reparametrization degrees of freedom. As in two dimensions one assumes that

$$\int \mathcal{D}[g] \rightarrow \sum_{\mathcal{T}} \frac{1}{\sigma} \quad (3.3)$$

defines the measure in a sensible way. The symmetry factor σ , a discrete remnant of the reparametrization group, is important mainly for small manifolds because the typical large manifold is not symmetric. In the following we will drop this factor.

Before one can define gravity using the piecewise linear metric defined above one has to discretize the Einstein Hilbert action (1.29). The cosmological term, which is the invariant D -volume of the manifold is rewritten as the sum of the volumes of the D -simplices the manifold is built from :

$$\int d^D \xi \sqrt{g} \rightarrow \sum_{D\text{-simplices}} V_D = N_D V_D. \quad (3.4)$$

To define the curvature on the discrete lattice one uses the parallel transport of a vector on a closed loop on the manifold. In a curved continuous space, the vector V_a changes by

$$\Delta V_a = \frac{1}{2} R_{abc}^d V_d \oint x^c dx^b \quad (3.5)$$

On the discrete manifold one considers a closed loop α dual to a $D-2$ -subsimplex s on the manifold. The loop α connects the centers of the D -simplices S_i which have s as a common sub-simplex. By definition the space inside the S_i is flat, $\Delta V_a = 0$ on these parts. However when α passes through a $(D-1)$ face the orientation of V_a changes by the deficit angle

$$\Theta_D = \arccos \left(\frac{1}{D} \right) \quad (3.6)$$

in the plane orthogonal to s . The rotation of S_a on the closed loop α dual to s is therefore described by a single angle

$$R_s = 2\pi - o(s)\Theta_D, \quad (3.7)$$

which we assign to s . The order $o(s)$ is the number of D -simplices which contain s as a common sub-simplex. The integrated curvature is a sum over all $(D-2)$ simplices s contained in the manifold :

$$\frac{1}{G_N} \int d^D \xi \sqrt{|g|} R \rightarrow \sum_s 2\pi - o(s)\Theta_D \propto c_D N_{D-2} - \frac{D(D+1)}{2} N_D \quad (3.8)$$

In deriving this we used the fact that a D -simplex has $\frac{D(D+1)}{2}$ $(D-2)$ sub-simplices and introduced the average order

$$c_d = \frac{2\pi}{\Theta_D} \quad (3.9)$$

of the s in flat space. For example in two dimensions one has $c_2 = 6$, the order of all vertices s in the triangulation of a flat surface is $o(s) = 6$. In higher dimensions there does not exist a triangulation of flat space, which is reflected by the fact that c_d is non-integer for $D > 2$. Nonetheless one can ask for the average order of a vertex in a hypothetical flat triangulation.

One gets the discrete Einstein Hilbert action by collecting (3.4) and (3.8)

$$S = \kappa_D N_D - \kappa_{D-2} N_{D-2}, \quad (3.10)$$

where the coupling κ_{D-2} is proportional to the inverse Newton constant G and κ_D is a linear combination of $1/G$ and the cosmological constant Λ . One can consider other terms in the action as well. For example in [58] the model with a curvature squared term was analyzed, this term, however, does not induce a different critical behavior.

The grand canonical partition function is defined as

$$\mathcal{Z}(\kappa_{D-2}, \kappa_D) = \sum_{\mathcal{T}} \exp(-\kappa_D N_D + \kappa_{D-2} N_{D-2}) = \sum_{N_D} \exp(-\kappa_D N_D) Z(\kappa_{D-2}, N_D) \quad (3.11)$$

where the sum runs over D -dimensional simplicial manifolds \mathcal{T} with fixed edges length a and fixed topology. The canonical partition function is defined as

$$Z(\kappa_{D-2}, N_D) = \sum_{\mathcal{T}_{N_D}} \exp(\kappa_{D-2} N_{D-2}), \quad (3.12)$$

where the sum runs over four dimensional simplicial manifolds \mathcal{T}_{N_D} with N_D four-simplices and fixed topology.

We want to close this section with a summary of the results obtained for the four dimensional model. The most important question, namely whether or not the partition function (3.11) is well defined has been disputed. The exponential $\exp(-\kappa_4 N_4)$ can prevent (3.11) from diverging only if the number of simplicial manifolds $\mathcal{N}(N_4)$ is exponential bounded. The numerical evidence is in favor of the existence of this bound [59, 60, 61]. Recently also an analytic argument [62] was given for this. The bound defines a critical line $\kappa_4^c(\kappa_2)$ drawn as the solid line in the phase diagram figure 3.1. For $\kappa_4 < \kappa_4^c(\kappa_2)$ eq. (3.11) diverges and the model is undefined. The continuum limit is taken by approaching the critical line from above, $\kappa_4 \rightarrow \kappa_4^{c+}$.

Numerically one finds two phases [55, 63]. The strong coupling phase is dominated by highly connected manifolds with very large, possible infinite, internal Hausdorff-dimension. The dominating geometries in the weak coupling phase have the structure of branched polymers. The internal Hausdorff dimension is $d_h = 2$, the entropy exponent $\gamma = \frac{1}{2}$ in this phase. For the model coupled to matter fields

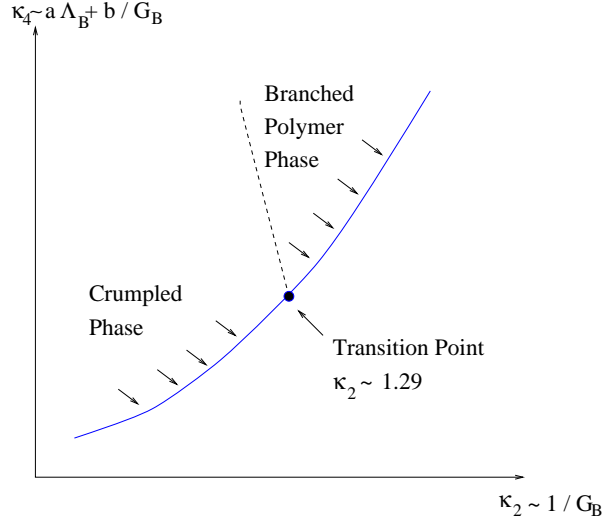


Figure 3.1: The phase diagram of four dimensional simplicial quantum gravity without matter.

investigated so far [64, 65, 66] only a renormalization of the coupling-constants was observed.

The strong coupling phase is dominated by two singular vertices [67, 68]. By singular we mean that the local volume assigned to these vertices is a finite fraction of the total volume in the thermodynamical limit; i.e. the local volume grows linear with N_4 . The appearance of these singular vertices can be understood in a constrained mean-field theory [70]. The two singular vertices are joined together by a sub-singular link l ; its local volume grows like $N_4^{2/3}$. The two phases are separated by a first order phase transition [50], [51] at $\kappa_2 \approx 1.29$. The singular structure which dominates the crumpled phase dissolves at this transition. On small lattices the transition actually appears in two steps [71, 72, 73]. Coming from the crumpled phase the sub-singular link disappears first. In the next step the singular vertices dissolve. For large volumes these sub-transitions seem to merge [73].

3.3 Topology

3.3.1 Introduction

One of the open questions in quantum gravity in dimensions larger than two concerns the role of topological excitations. It seems a bit artificial to fix the topology by hand, which is what is usually done in the simulations. The situation in four dimensions is complicated by the fact that as of date no topological classification of four manifolds is known. Allowing an arbitrary topology will result in a very complicated structure at the Planck scale because curvature fluctuations become larger at smaller scales [74]. In [75] it was estimated that the dominant contribution to the path integral would come from space-times where the Euler character χ is of the order of the volume of the space-time in Planck units. Such a configuration with many holes is commonly called a space-time foam.

In [76] a tensor model similar to the matrix model (section 1.5) was considered, which generates pseudo-manifolds with fluctuating topologies. It was shown that for large couplings κ the pseudo-manifold decomposes in very small connected components while in the weak coupling phase there is only one connected component. However, it is not obvious how these pseudo-manifolds, which have now unique local internal dimension, are related to four dimensional space-time.

In this work check numerically, if topology fluctuations are dynamically suppressed. In a theory containing topology fluctuations only those topologies contribute to the sum in the thermodynamic limit, which maximize the extensive part of the free energy. Other contributions are exponentially suppressed. Two dimensional quantum gravity provides us with an example of to define a theory which contains topological excitations. In the double scaling limit which we discussed in section 1.5, *all* topological excitations are present. The physical reason is that the leading contribution to the free energy is independent of the topology. If one believes that *all* topological excitations are present also in four dimensions the bulk volume contribution to the free energy should also be independent of the topology. We investigate numerically three different topologies and show that in these cases, up to the leading order, the free energy does not depend on the topology. We observe a topology dependence in the next to leading order. We study those volume corrections and analyze their kinematic sources.

3.3.2 Model and methods

Given the canonical partition function (3.12), we define the intensive free energy as

$$f(\kappa_2) = \lim_{N_4 \rightarrow \infty} \frac{1}{N_4} \log Z(\kappa_2, N_4). \quad (3.13)$$

For large N_4 the free energy is assumed to have the form:

$$F(\kappa_2, N_4) = N_4 f(\kappa_2) + \delta(\kappa_2, N_4), \quad (3.14)$$

where the function δ is a finite size correction, i.e. for any κ_2

$$\lim_{N_4 \rightarrow \infty} \frac{\delta(\kappa_2, N_4)}{N_4} = 0. \quad (3.15)$$

The derivatives of the free energy are convenient to recover some basic properties of the theory. The action density

$$r(\kappa_2, N_4) = \frac{1}{N_4} \frac{\partial F}{\partial \kappa_2} = \frac{\langle N_2 \rangle}{N_4} \quad (3.16)$$

is normalized such that it becomes an intensive quantity in the thermodynamic limit. We call the derivative with respect to N_4 ,

$$\tilde{\kappa}_4(\kappa_2, N_4) = \frac{\partial F}{\partial N_4}. \quad (3.17)$$

the pseudo-critical value of the parameter κ_4 . This definition differs slightly from the one proposed in [59]. This quantity is a measure of finite size dependence of the free energy, i.e. of how fast it approaches the thermodynamic limit $\tilde{\kappa}_4 \rightarrow \tilde{\kappa}_4(\kappa_2)$ for $N_4 \rightarrow \infty$. In this limit the value $\tilde{\kappa}_4(\kappa_2)$ defines the critical line of the model corresponding to the radius of convergence of the series (3.11).

The pseudo-critical value $\tilde{\kappa}_4(\kappa_2, N_4)$ is related to the action density by

$$\frac{\partial \tilde{\kappa}_4}{\partial \kappa_2} = r + N_4 \frac{\partial r}{\partial N_4} \quad (3.18)$$

where the second term goes to zero when N_4 goes to infinity. Therefore the critical parameter $\tilde{\kappa}_4$ becomes an integral of r in the thermodynamic limit. Thus, if r is independent of the topology so is $\tilde{\kappa}_4$ unless the integration constant depends on the topology. To fix the integration constant it is sufficient to measure $\tilde{\kappa}_4$ for only one particular value of κ_2 .

The action density (3.16), the normalized average number of triangles on the manifold, is a standard observable which is easily accessible in canonical simulations. For the pseudo-critical value $\tilde{\kappa}_4$ (3.17) more unconventional methods are required. The baby universe method, which we used in the context with hyper-cubic random surfaces to extract the next to leading correction, unfortunately works only in the elongated phase. Following [59], we adopt here a more general method based on grand-canonical simulations, which works equally well in all phases. We use multi-canonical simulations with a potential $U(N_4)$. From the volume fluctuation one can extract the volume dependence of $\tilde{\kappa}_4$. We expect the quantity $\partial F / \partial N_4$, which we want to measure, to smoothly approach the function $f(\kappa_2)$. The freedom one has in choosing the potential U can be used to minimize the statistical error of the observable. A Gaussian potential controlling fluctuations around a fixed volume V_4 is well suited for this problem [59] :

$$U = \kappa_4 N_4 + \frac{\gamma}{2} (N_4 - V_4)^2 \quad (3.19)$$

but other potentials can be used as well [55]. With this potential the multi-canonical partition function reads :

$$\mathcal{Z} = \sum_T e^{\kappa_2 N_2 - U(N_4)} = \sum_{N_4} e^{F(\kappa_2, N_4) - \kappa_4 N_4 - \frac{\gamma}{2} (N_4 - V_4)^2} \quad (3.20)$$

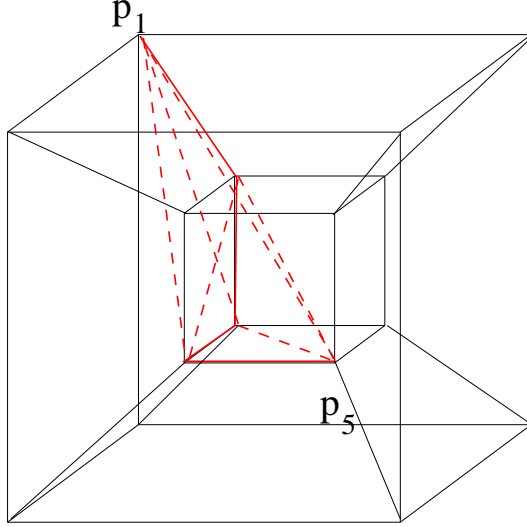


Figure 3.2: A four tetrahedron built into a four dimensional hyper-cube.

The distribution of the volume N_4 becomes Gaussian around $N_4 = V_4$ if one expands $F(\kappa_2, N_4)$ around this point

$$P(x = N_4 - V_4) \sim \exp\left(-\frac{\Gamma}{2}(x - x_0)^2 + \dots\right) \quad (3.21)$$

The parameters Γ and x_0 are related to F and U by:

$$\Gamma = \gamma - \partial^2 F / \partial V_4^2, \quad x_0 = (\partial F / \partial V_4 - \kappa_4) / \Gamma. \quad (3.22)$$

Both quantities can be measured in the simulations, by tuning κ_4 close to the derivative $\partial F / \partial V_4$ and choosing γ much larger than the second derivative $\partial^2 F / \partial V_4^2$. The parameter Γ can be extracted from the width of the distribution and x_0 from the shift of the maximum from $N_4 = V_4$. This gives an estimate for the pseudo-critical coupling at V_4 :

$$\tilde{\kappa}_4 = \partial F / \partial V_4 = \Gamma x_0 + \kappa_4. \quad (3.23)$$

In this formula, κ_4 is the coupling used in the simulation from which x_0 and Γ were extracted. The estimator can be improved by minimizing x_0 . This can be done recursively by replacing κ_4 by $\tilde{\kappa}_4$ in subsequent simulations.

The value for the multi-canonical coupling γ should be chosen large enough so that the volume fluctuations are small compared to the scale of change of $F(N_4, \kappa_2)$. On the other hand, the algorithm used in the simulation is grand canonical and requires volume fluctuations for ergodicity. Therefore γ should be small enough to allow sufficient N_4 fluctuations. We checked that for $\gamma = 0.0001$, Γ computed from the width of the distribution $\Gamma = 1 / \sqrt{\sigma^2(N_4)}$, i.e. $\Delta N_4 = 100$, was equal to γ within the error bars. From (3.22) it follows that $\gamma \gg \partial^2 F / \partial V_4^2$. Therefore the free energy changes very slowly across the range of the N_4 distribution width as needed for the approximation (3.21) to be valid.

Because the local moves [77] used in the Monte Carlo simulation preserve the topology t of the manifold, t is given by the topology of the starting configuration.

In our simulation we simulated a spherical S^4 topology and two different tori, namely $S^3 \times S^1$ and $S^1 \times S^1 \times S^1 \times S^1$.

The starting configuration for the sphere is, as usual, the $4d$ -boundary of a 5-simplex. The $S^1 \times S^1 \times S^1 \times S^1$ manifold can be built out of the regular 3^4 square torus by dividing each elementary $4d$ -cube into 4-simplices in the following way. For each cube we mark two points, $p_1 = (0, 0, 0, 0)$ and $p_5 = (1, 1, 1, 1)$, lying on the opposite ends of the main diagonal and connect them by one of the shortest paths going along the edges of the cube. The shortest path goes through 4 edges, each in a different direction, and through three points, say p_1, p_2, p_3 . There are 24 such paths. Each set of points p_0, p_1, p_2, p_3, p_4 forms a 4-simplex. In figure 3.2 we show as an example one four-simplex (red) built into a four dimensional cube obtained with this procedure. The dashed lines are additional diagonals which have to be inserted to complete the four-tetrahedron. The manifold condition requires that no vertex be connected to itself. Therefore one has to glue together 4 cubes in all four directions. The starting configuration therefore contains $3^4 * 24 = 1944$ four simplices.

The manifold $S^3 \times S^1$ can be produced from a spherical manifold by taking away two separate 4-simplices and gluing together the boundaries b_1, b_2 created by removing the two 4-simplices. However, two vertices in a 4d simplicial manifold may have at most one common link. To avoid the creation of a double connection in the gluing process, the distance between the vertices on b_1 to those on b_2 has to be at least three links. One can ensure this, without going through a tedious check, by gluing cyclically together three copies of the original (spherical) manifold, i.e. $b_1/b'_2, b'_1/b''_2, b''_1/b_2$. The (double-) prime is used to distinguish the different copies. The boundaries b_1, b_2 are chosen such that they have no common vertex.

3.3.3 Numerical results

We have performed simulations with $N_4 = 4000, 8000, 16000, 32000, 64000$ for the three topologies discussed above. The explicit form of the sub-leading correction $\delta(\kappa_2, N_4)$ depends on the phase where the measurement is taken. The elongated phase of simplicial gravity is dominated by branched polymers [55, 71, 78]. This means that in the large volume limit one can use the ansatz

$$F(\kappa_2, N_4) = N_4 f_0(\kappa_2) + (\gamma - 3) \log N_4 + f_1(\kappa_2) + \mathcal{O}\left(\frac{1}{N_4}\right) \quad (3.24)$$

for the free energy. The correction coefficient γ is assumed to depend only on the genus g of the manifold. The logarithmic corrections disappear for the action density r eq. (3.16)

$$r = \frac{1}{N_4} \frac{\partial F(\kappa_2, N_4)}{\partial \kappa_2} = f'_0(\kappa_2) + \frac{f'_1(\kappa_2)}{N_4}. \quad (3.25)$$

Therefore one should take the next order corrections $1/N_4$ into account. We will show that they appear for purely kinematic reasons. Consider the limit of large positive κ_2 in which only manifolds maximizing N_2 contribute to the sum (3.11). Such triangulations can be obtained from barycentric subdivisions (3.54) of 4-simplices

applied successively to a minimal starting configuration, possibly mixed with micro-canonical transformations (3.74), which do not change N_2 and N_4 . By the minimal configuration we mean the minimal volume triangulation which maximizes N_2 . For the barycentric subdivisions one gets the relation $N_2 = 5/2N_4 + c^0$, where the constant

$$c^0 = N_2^0 - 5/2N_4^0 \quad (3.26)$$

characterizes the initial minimal configuration. The number of triangles N_2 is related to the action density $r = N_2/N_4 = 5/2 + c^0/N_4$. This means that the constant c^0 leads to $1/N_4$ corrections of the action density. The contributions to the sum (3.11) from triangulations built from non-minimal ones (i.e. smaller N_2) are suppressed exponentially by $\exp -\kappa_2(c^0 - c)$, where c characterizes the non minimal starting configuration with $c(\kappa_2) < c^0$.

The minimal configuration for the sphere, the surface of a 5-simplex, is known and hence c^0 is known. For the two toroidal geometries we find the minimal configuration numerically. We use our Monte Carlo code in a cooling procedure, in which we increase κ_4 , to decrease N_4 , and increase κ_2 , to maximize N_2 . In practice we have to increase κ_2 slowly compared to κ_4 , because increasing κ_2 also increases pseudo-critical coupling $\tilde{\kappa}_4(\kappa_2)$. For the topologies we studied, we found the following minimal configurations :

$$\begin{aligned} S^4 & : N_4^0 = 6, \quad N_2^0 = 20 \quad \Rightarrow c^0 = 5, \\ S^3 \times S^1 & : N_4^0 = 110, \quad N_2^0 = 44 \quad \Rightarrow c^0 = 0, \\ S^1 \times S^1 \times S^1 \times S^1 & : N_4^0 = 704, \quad N_2^0 = 1472 \quad \Rightarrow c^0 = 288. \end{aligned} \quad (3.27)$$

For the manifold $S^3 \times S^1$ the finite volume correction $1/N_4$ is not present at all. It is also very difficult to detect them for the sphere S^4 because $c^0 = 5$ is very small compared to the volume N_4 used in the simulation. For the torus $S^1 \times S^1 \times S^1 \times S^1$ the corrections are, however, two orders of magnitude larger and measurable in the volume range used in the simulations. This estimate of the $1/N_4$ effect is exact only for infinite positive κ_2 but one expects it to work, although with a slowly varying coefficient $c(\kappa_2)$, in the entire elongated phase.

In figure 3.3 we show the action density r measured in the elongated phase for $\kappa_2 = 2.0$ against $1/N_4$. In the same figure we display the curve $r_\infty + c^0/N_4$ with $c^0 = 288$ and $r_\infty = 2.482$ which fits the data points very well. Note that that r_∞ does not depend on the topology.

For the pseudo-critical coupling $\tilde{\kappa}_4$ we observe, with the statistics available, no volume and/or topology dependence either. We find $\tilde{\kappa}_4^\infty = 5.659(4)$ for $\kappa_2 = 2.0$ in the infinite volume limit. This is compatible with the ansatz

$$\tilde{\kappa}_4(\kappa_2, N_4) = f_0(\kappa_2) + \frac{\gamma - 3}{N_4}, \quad (3.28)$$

because γ is known to be of order $\mathcal{O}(1)$. With the method used, the correction could only be separated from the statistical noise with an disproportionate amount of computer time.

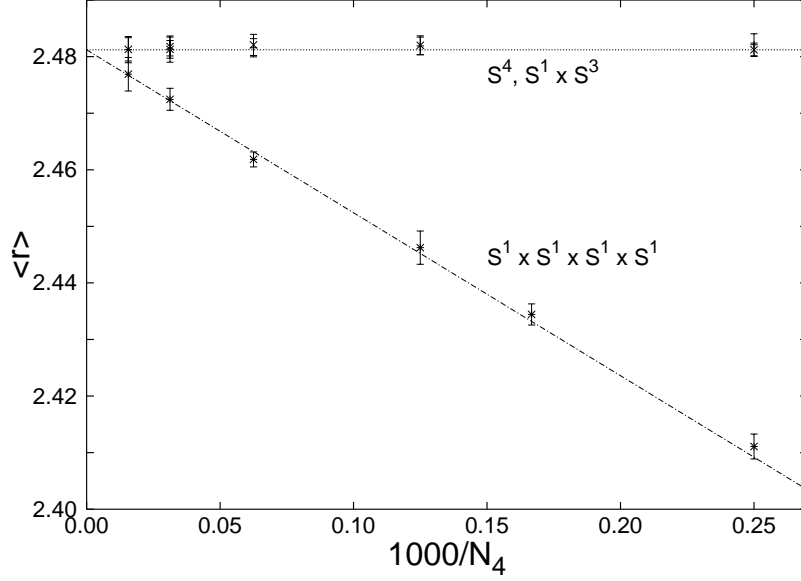


Figure 3.3: The volume dependence of the action density r for three different topologies in the elongated phase at $\kappa_2 = 2.0$

In the crumpled phase we use a power-law ansatz

$$F(\kappa_2, N_4) = N_4 f_0(\kappa_2) + f_1(\kappa_2) N_4^\delta \quad (3.29)$$

Taking the derivative with respect to N_4 one gets:

$$\tilde{\kappa}_4(\kappa_2, N_4) = f_0(\kappa_2) + \delta f_1(\kappa_2) N_4^{\delta-1}. \quad (3.30)$$

For the action density (3.16) one finds

$$r = f'_0(\kappa_2) + f'_1(\kappa_2) N_4^{\delta-1} \quad (3.31)$$

We checked this ansatz by fitting our numerical data for $r(N_4)$ to eq. (3.31):

Topology	δ	$r^\infty = f'_0$	$\log(f'_1)$	χ^2/dof
S^4	0.5 (2)	2.039 (+0.010 / -0.013)	1.9 (1.3)	0.78
$(S^1)^4$	0.6 (2)	2.028 (+0.008 / -0.016)	1.0 (0.9)	0.87
$S^1 \times S^3$	0.5 (2)	2.038 (+0.010 / -0.021)	1.8 (1.3)	0.31

and $\kappa_4(N_4)$ to (3.30):

Topology	δ	$\kappa_4^\infty = f_0$	$\log(\delta f_1)$	χ^2/dof
S^4	0.6 (2)	1.20 (2)	1.4 (1.3)	0.22
$(S^1)^4$	0.6 (3)	1.20 (2)	1.4 (1.5)	0.10
$S^1 \times S^3$	0.6 (2)	1.20 (2)	1.4 (1.3)	0.18

In the tables we give the logarithms of f'_1 and δf_1 since these have approximately symmetric errors. One can see that the values do not depend, within errors, on

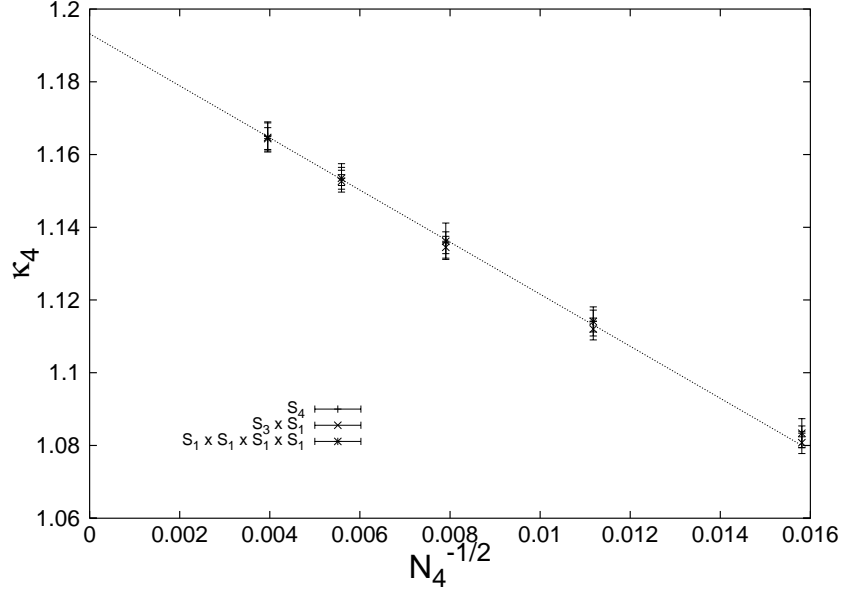


Figure 3.4: The volume dependence of the critical κ_4 for three different topologies in the crumpled phase at $\kappa_2 = 0.0$

topology. In figure 3.4 we show the numerical data for κ_4 for the three topologies and $\delta = 0.5$.

The source of the volume correction in this phase can be understood by looking at the typical configurations which dominate the ensemble for large negative κ_2 . These configurations minimize the free energy and therefore have for fixed volume the minimal number of vertices, and thus also the minimal number of triangles. In three dimensions such configurations were constructed in [57]. The generalization to the four dimensional case is obvious. One starts with a $2d$ triangulation of the sphere with t triangles. At each triangle one builds a $4d$ -pancake neighborhood from q 4-simplices lying around the triangle in such a way that the links opposite to this triangle form a circle. An opposite link is defined as a link which does not share a common vertex with the triangle. The next step is to put neighboring pancakes together by identifying these circles with the $3d$ faces of the neighboring pancakes. Each pancake has three such faces which lie between the circle and an edge of the basic triangle. It also has three neighboring pancakes. After this step one gets an S^4 sphere with $t * q$ 4-simplices and $2 + t/2 + q$ vertices. The highest connectivity $N_4 \sim (N_0 - 2)^2/2$ is reached when $t = 2q$. The number N_2 of triangles can be constructed from this as a function of N_4 making use of the Dehn-Somerville relations (3.1). Inserting the result into (3.16) one finds $r \propto 1/\sqrt{(N_4)}$ i.e. $\delta = 0.5$ for these configurations.

In [50], evidence was given that for spherical topology the phase transition is of first order. We could observe flip-flops in the action density for the two tori as well. This seems to show that the transition in these cases is of first order as well.

3.3.4 Discussion

We have investigated the behavior of the curvature and the entropy density for three different topologies in four dimensional simplicial quantum gravity. We concentrated on two κ_2 values, one deep in the crumpled phase and another value in the elongated phase. In both cases the value of the entropy density $\kappa_4^c(\kappa_2)$ and the curvature were independent on the topology in the large volume limit. We have shown that κ_4^c is an integral of the curvature. The observation that κ_4^c is independent from the topology in the two phases of the model therefore suggests that the curvature and the entropy density do not depend on the topology for all κ_2 in the thermodynamical limit. This gives support to the conjecture that it is possible to define, similar to the double scaling limit in two dimensions, a scaling with coherent contributions from all topological excitations. We can, however, not fully exclude that in the transition region the curvature and hence κ_4 depend on the topology but this, by chance, cancels out after integrating over this region; this seems very unlikely, though.

Our result furthermore supports the conjecture that the entropic bound exists. This question was recently discussed in the literature [79, 80, 81]. The value of the entropy density κ_4 can be compared with the estimates given in [62], based on a summation over curvature assignments. This estimate, does, however, not directly give results in agreement with our numerical data for $\tilde{\kappa}_4$. We conclude that the mapping from the entropy of curvature assignments to the entropy of four-manifolds, which is a basis for the calculations in [62], is too simple to capture fully the behavior in the $4D$ approach.

We have analyzed the finite size effects observed for the model. We gave kinematic arguments which explain the leading correction very well.

3.4 Simplicial quantum gravity coupled to gauge matter fields

3.4.1 Introduction

As mentioned in the introduction, the dominating geometries in the two phases found in four dimensional simplicial quantum gravity do not describe extended four dimensional structures. This, however, is required for the model to describe the large distance behavior of space-time. The phase transition is of first order. Therefore one can not take the continuum limit at this point. In this situation it is sensible trying to insert terms into the action which cure these problems.

In the crumpled phase, for example, one may try to suppress configurations with large order $o(t)$, i.e. singular vertices, by adding a term

$$- \alpha \log \sum_t o(t) \tag{3.32}$$

to the action. We have simulated the model with this term. We found, however, almost no back-reaction of the gravity sector on this term. Both phases survive. At the transition one finds flip-flops in the time-series of N_0 which indicates that the transition is still first order.

The branched polymer behavior observed in the elongated phase in fact plagues many theories of random geometries in all dimensions. One phase of the hypercubic random surface model investigated in this thesis is a example of such a theory. On the other hand, pure gravity in $D = 2$ dimensions is in the non-trivial Liouville phase with string susceptibility exponent $\gamma < 0$. In this phase it is possible to define a sensible continuum limit. The branched polymer behavior returns, however, if one couples matter with central charge $c > 1$ to two dimensional quantum gravity. In [82, 83, 84] a heuristic argument was given to explain this behavior: When c becomes larger than the $c_b = 1$ 'barrier' metric singularities condense. The argument is similar to the Berezenskii-Kosterlitz-Thouless [85, 86] argument for a transition in the 2-D $x - y$ model. It relies on the construction of singular configurations ('spikes') and the observation that the action for such configurations grows logarithmically with the infrared cut-off. From the continuum methods and the known dynamics of the conformal factor (1.23) it is known that the action for a spike

$$S(c) \propto (26 - c) \log\left(\frac{L}{a}\right) \tag{3.33}$$

becomes smaller with larger c . The entropy $E \propto \log(L/a)$ of putting spike onto the surface on the other hand grows logarithmically with the linear extent L of the surface. It was shown that for $c > 1$ the entropy E becomes larger than the action $S(c)$ and the creation of spikes is favored.

In [87] it was suggested that a similar phenomenon might occur in four dimensions. An effective action for the conformal factor in four dimensions was derived in [88, 89]. As in two dimensions the action for a spike grows logarithmically with the linear extent L :

$$S_E[\sigma_s] = \frac{1}{2} Q^2 q^2 \log\left(\frac{L}{a}\right). \tag{3.34}$$

The coupling

$$Q^2 = \frac{1}{180}(N_s + \frac{11}{2}N_{WF} + 62N_V - 28) + Q_{grav}^2 \quad (3.35)$$

depends on the numbers N_s of scalar fields, N_{WF} of Weyl fermions and N_V vector fields. The term Q_{grav}^2 describes the (unknown) contribution of spin-2 gravitons. The only negative contribution -28 comes from the conformal factor itself. The most interesting point about this result is that, differently from the two dimensional case, the effective action becomes larger when one adds matter to the model. In other words, putting matter into the model stabilizes the model and suppresses spikes. This suggests that in the absence of matter fields quantum gravity has no sensible vacuum, but this instability is lifted when the number of matter fields is large enough.

It should be emphasized that in four dimensions the action (3.34) for spikes can not be derived rigorously, because it is not clear how transverse excitations of the metric should be treated. Nevertheless the conjecture above makes is very interesting to investigate the influence of matter on the geometry in $4d$ simplicial quantum gravity. It may also explain why in earlier investigations [64, 65, 66] no non-trivial effects induced by the matter have been observed. In the framework of [52] it was shown that spikes are dominant if $Q^2 < 8/q^2$. It may be that in the earlier investigations not enough matter fields were introduced so that Q^2 was still too small.

3.4.2 The model

From (3.35) one can read off that the strongest effect on the geometry is caused by the number of vector fields. Therefore we study a model of continuous vector gauge fields coupled to 4d simplicial gravity. Specifically we consider non-compact $U(1)$ gauge fields $A(l_{ab})$ living on the links l_{ab} of the simplicial manifold and $A(l_{ab}) = -A(l_{ba})$. The sum in the action

$$S_M = \sum_{t_{abc}} o(t_{abc}) [A(l_{ab}) + A(l_{bc}) + A(l_{ca})]^2 \quad (3.36)$$

extends over all triangles t_{abc} . The order $o(t_{abc})$ is equal to the number of four simplices which contain t_{abc} and is proportional to the local volume assigned to the triangle. This factor appears to mimic the factor \sqrt{g} which appears in a covariant action. There is no need to introduce a coupling in front of the sum because the action has a Gaussian form.

In the model with n gauge fields we put n replicas of the matter field on the dynamic geometry. The action

$$S_M^{(n)} = \sum_{i=1}^n {}^{(i)}S_M \quad (3.37)$$

is the sum of the one field actions (3.36) with ${}^{(i)}S_M = S_M$. Note that there is no explicit interaction between the replicas of the model. On a fixed lattice such a

model is trivial, the behavior of a single replica remains unchanged. On a dynamic lattice, however, the systems are coupled by the back-reaction of the dynamical geometry on the matter fields.

The action for the combined system of gravity and matter contains, besides $S_M^{(n)}$, two more terms. The contribution of the gravity sector is given by the discrete Einstein-Hilbert action (3.10) which in four dimensions reads

$$S_G = -\kappa_2 N_2 + \kappa_4 N_4. \quad (3.38)$$

where N_k denotes the number of k -simplices. The third term is present for technical reasons. The algorithm in the simulation is inherently grand canonical and requires volume fluctuations to satisfy ergodicity. We use the multi-canonical potential (3.19) to simulate a pseudo-canonical ensemble with almost fixed $N_4 \approx N_4^{(0)}$. Measurements are taken only if $N_4 = N_4^{(0)}$. The coupling κ_4 is tuned so that $\overline{N_4} = N_4$.

The model is defined by the partition function

$$Z(\kappa_2, \bar{N}_4) = \sum_T W(T) \int' \prod_{i=1}^n \left(\prod_{l \in T} dA^{(i)}(l) \right) e^{-S_G - S_M^{(n)} - \frac{\delta}{2}(N_4 - \bar{N}_4)^2}. \quad (3.39)$$

The sum extends over all distinct four dimensional simplicial manifolds T and $W(T)$ is the symmetry factor taking care of equivalent re-labelings of vertices. The prime at the integral indicates that the zero modes of the gauge field are not integrated.

3.4.3 The strong coupling expansion

The first few terms of the strong coupling expansion can be used to estimate the exponent γ [90]. We used our code without matter fields to identify diagrams up to $N_4 = 30$ and calculated the symmetry factor σ for the diagrams by counting the number of invariant re-labelings². Without matter the weight for a diagram is $W = 1/\sigma$. To debug our computer code we identified the diagrams with $N_4 \leq 18$ by inspection and verified that the theoretical and numerical distributions governed by the symmetry factor agree.

For the strong coupling expansion of the model with matter-field we have to calculate the weight induced by the matter. The Gaussian integration which excludes zero-modes over one species of fields leads to a determinant ρ . As the n replicas of the field interact only indirect via the back-reaction of the gravity and have no explicit interaction term in the action it is sufficient to calculate the weights ρ_M for one field. The n -field weight is

$$W^{(n)} = \rho_M^n / \sigma. \quad (3.40)$$

The weights ρ_M were calculated using Maple. In table (3.1) we summarize the results obtained with this procedure.

The series was then analyzed with the ratio method [90] to extract the exponent γ . In the upper plot in figure 3.5 we show the behavior of γ as a function κ_2

²For a detailed discussion of this method see section 2.5.1.

N_4	N_0	N_g	$W^{(0)}$	$W^{(1)}$	$W^{(3)_3}$
6	6	1	1	1	1
10	7	1	3	0.097638467...	$1.03423... \times 10^{-4}$
12	7	1	5	0.030058406...	$1.08632... \times 10^{-6}$
14	8	1	15	0.018550484...	$2.83715... \times 10^{-8}$
16	8	2	255/4	0.015777808...	$9.68553... \times 10^{-10}$
18	8	3	110	0.005500465...	$1.38182... \times 10^{-11}$
	9	3	95	0.004759295...	$1.19996... \times 10^{-11}$
20	8	2	225	0.002512817...	$3.15034... \times 10^{-13}$
	9	7	693	0.007291315...	$8.14758... \times 10^{-13}$
22	9	15	2460	0.005728290...	$3.27573... \times 10^{-14}$
	10	7	690	0.001447804...	$6.46761... \times 10^{-15}$
24	9	13	16365/2	0.004226212...	$1.17586... \times 10^{-15}$
	10	34	14625/2	0.003378959...	$7.45244... \times 10^{-16}$
26	9	50	17865	0.001946262...	$2.34367... \times 10^{-17}$
	10	124	39645	0.003936950...	$3.97116... \times 10^{-17}$
	11	30	5481	0.000491334...	$4.06700... \times 10^{-18}$
28	9	89	291555/7	0.001058334...	$6.96159... \times 10^{-19}$
	10	415	182820	0.004119603...	$2.16619... \times 10^{-18}$
	11	217	77057	0.001534637...	$6.33995... \times 10^{-19}$
30	9	139	73860	0.000457581...	$1.78973... \times 10^{-20}$
	10	1276	672821	0.003427165...	$9.13722... \times 10^{-20}$
	11	1208	564000	0.002507268...	$5.17157... \times 10^{-20}$
	12	143	46376	0.000179907...	$2.84432... \times 10^{-21}$

Table 3.1: The number of different graphs N_g , for a fixed volume N_4 and fixed number of vertices N_0 and the corresponding weights $W_{N_V}(N_4, N_0)$ for 0, 1 and 3 vector fields. All weights are normalized with the value at $N_4 = 6$.

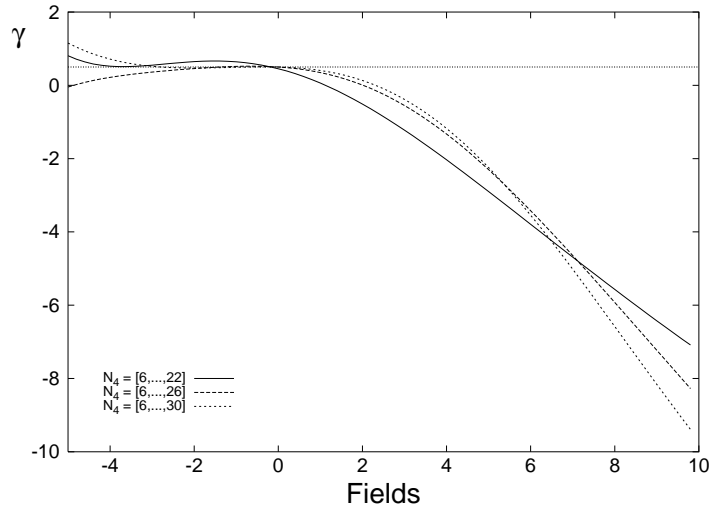
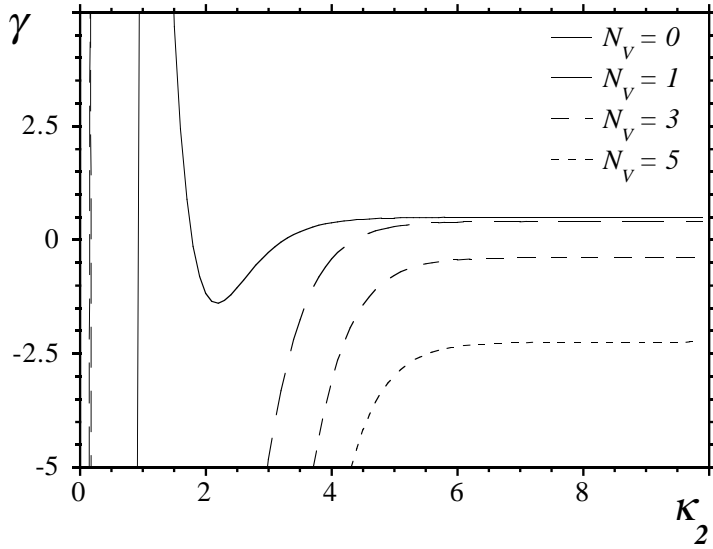


Figure 3.5: (a) Variations of γ with κ_2 , for 0, 1, 3, and 5 vector fields coupled to gravity. (b) Variation of γ with the number of fields for $\kappa_2 = 10.0$. These values are obtained using the ratio method to analyze the strong coupling series including terms corresponding to $N_4 = 6, 10, 14, 18, 22, 26$, and 30. The horizontal line in the lower diagram is at $\gamma = 0.5$, the exponent expected for pure gravity.

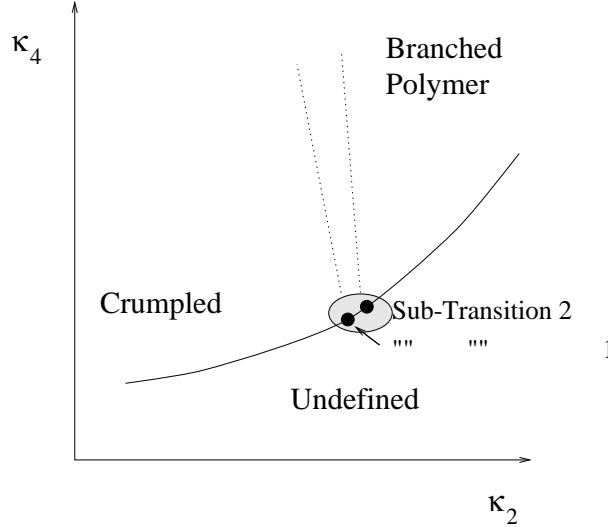


Figure 3.6: The phase diagram for the model with one vector field.

obtained with this method. For large κ_2 the susceptibility exponent γ tends to a constant value which becomes negative when the number of fields grows. For pure gravity one finds $\gamma = \frac{1}{2}$ as expected. For small enough κ_2 the exponent γ is large negative. In the intermediate region the results are unstable. This presumably indicates a phase transition in this range of the coupling κ_2 . In the lower plot we show the variation of γ as a function of the number of vector fields at $\kappa_2 = 10.0$, i.e. in the weak coupling phase. We used diagrams of size $[6, \dots, 22]$, $[6, \dots, 26]$ and $[6, \dots, 30]$ for the three different curves. One sees that they depend slightly on the size of the largest diagrams used in the series expansion, however they seem to converge for larger diagrams. This and the numerical results presented in the next section justify the assumption that the series expansion presented here describes correctly the qualitative behavior of the exponent γ .

3.4.4 Numerical results

The first question when analyzing a new model is about the phase diagram. The gauge fields investigated here introduce a new parameter into the model, namely the number n of fields. We have performed Monte Carlo simulations for the model with one and three vector fields. For the survey of the phase structure we use rather modest lattice sizes with no more than 16K four-simplices. It is known from the simulations of pure gravity that finite size effects are quite strong; for example the order of the phase transition for pure gravity reveals itself only for lattices larger than 32K. It is therefore clear that one has to be careful when drawing strong conclusions from the numerical data presented here. Nevertheless we believe that the qualitative picture obtained from the data is reliable. This is supported by the observation that the results are in good agreement with the strong coupling expansion.

In figure 3.6 we present the phase diagram found for one vector field. The model

diverges if $\kappa_4 < \kappa_4^c(\kappa_2)$ and the model is undefined. We observed no back-reaction in the strong coupling phase, which is still dominated by singular structures. Likewise, the weak coupling phase is still a branched polymer. In the transition region we observe two sub-transitions indicated by two peaks in the node susceptibility

$$\chi_0 = (\langle N_0^2 \rangle - \langle N_0 \rangle^2) / N_4. \quad (3.41)$$

The first sub-transition has a broad peak. With the statistical noise it is difficult to locate precisely the point of the transition. Therefore our data does not allow to judge if with growing volume the two transitions merge to the same critical coupling. They are presumably similar to the two sub-transitions observed for pure gravity on small lattices³, which do seem to merge [73].

The picture changes when we include three vector fields. We still find singular structures in the strong coupling phase, but the weak coupling phase has no longer a branched polymer behavior. The two phases are separated by a maximum of the node susceptibility at $\kappa_2 \approx 1.9$ which grow with the volume as seen in figure 3.7. To locate the critical coupling and understand the nature of the transition one needs better statistics and simulations for larger systems; this is in progress but it will, however, require several more months of CPU time.

The change in the geometry at roughly the same coupling where χ_0 has its maximum is, however, a strong indication that we observe a real transition. In plot (b) of figure 3.7 we show the difference between the orders of the most singular and the third most singular vertex $p_1 - p_3$. In the strong coupling phase the order of the first and second most singular vertices are roughly of the same order. They are separated by a large gap from the order of the other vertices. For larger κ_2 the order of these two vertices merge to the order of other vertices.

This means that there is no singular vertex in the weak coupling phase, as demonstrated by the scaling behaviour of the most singular vertex p_0 in figure 3.8 for $\kappa_2 = 4.5$. The local volume of this vertex grows sublinearly like $N_4^{3/4}$, i.e. a vanishing fraction of the total volume N_4 in the thermodynamical limit.

In the same plot (3.8) we show the scaling of the average distance between the simplices [91]:

$$\langle r_{ij} \rangle_{N_4} = \left\langle \sum_{r=0}^{\infty} r n(r) \right\rangle \sim N_4^{1/d_H}, \quad (3.42)$$

where $n(r)$ counts the number of simplices at a geodesic distance r from a marked simplex. With a fit to equation (3.42) we get for the Hausdorff dimension $d_h = 3.93(15)$. However, the data points do not lie on a straight line, presumably due to finite size effects. If we exclude the data point for the smallest volume $N_4 = 2000$ we get $d_h = 4.68(8)$.

We use the baby universe method [92] to measure the entropy exponent γ in the weak coupling phase. The method was explained for the hyper-cubic random surface model in section 2.3.2. Up to some technicalities the method is the same for the model discussed here. In table 3.2 we list the results obtained for three vector fields with this method for two values of κ_2 (4.5 and 6.0) and at different volumes.

³ See also the end of section 3.2

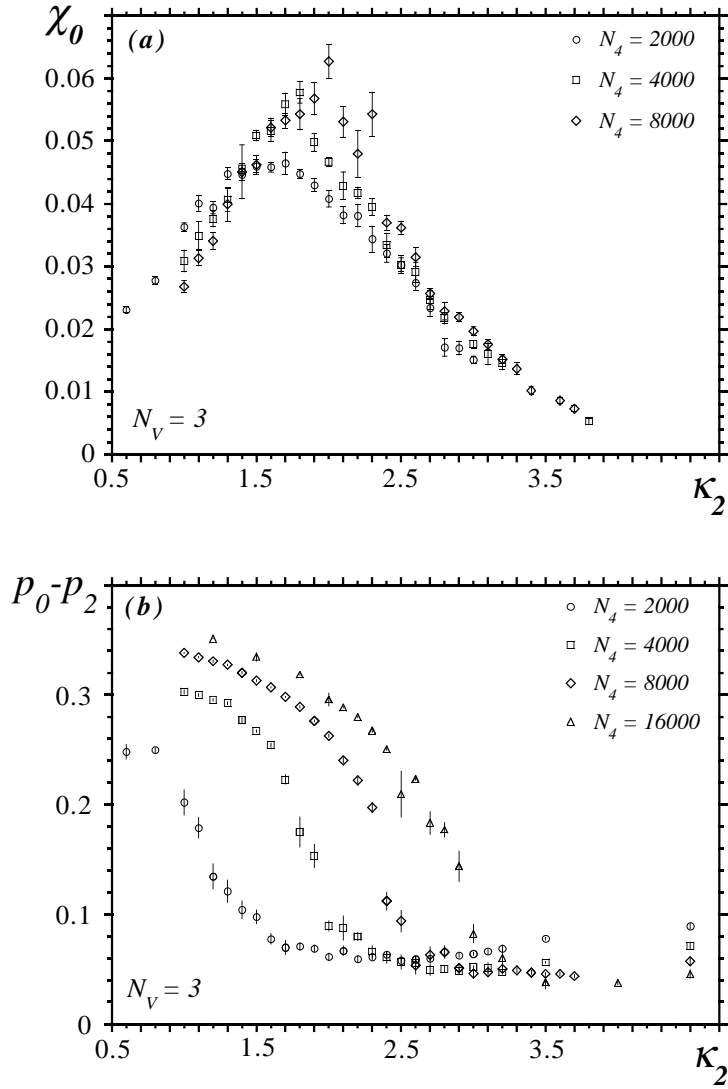


Figure 3.7: (a) The node susceptibility χ_0 , for three vector fields coupled to gravity, vs. κ_2 . For $N_4 = 16000$ the statistics is not sufficient for a reliable estimate of χ_0 . (b) The corresponding change in the difference between the orders of the first and of the third most singular vertex, p_0 and p_2 , normalized with the total volume N_4 .

N_4	$\kappa_2 = 4.5$	$\kappa_2 = 6.0$
2000	-0.22(2)	
4000	-0.18(3)	-0.17(4)
8000	-0.23(3)	
16000	-0.30(6)	-0.12(6)

Table 3.2: Measured values of the string susceptibility exponent γ in the weak coupling (large κ_2) phase for three vector fields

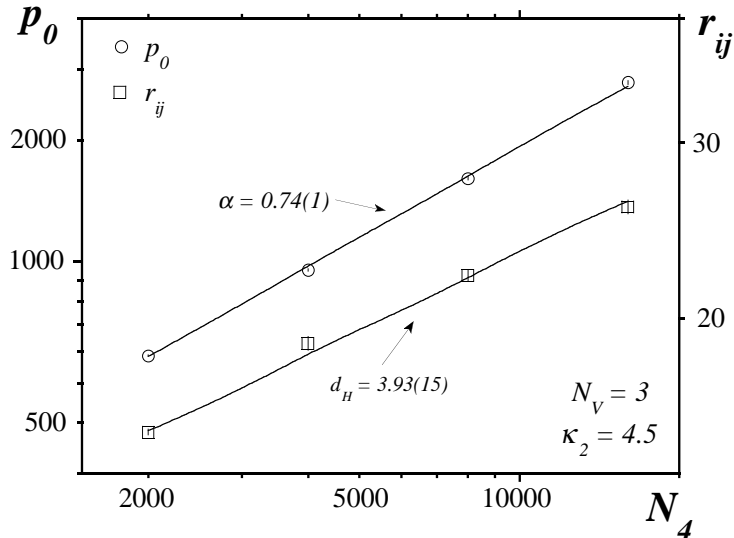


Figure 3.8: The scaling of both the largest vertex order p_0 and the average distance r_{ij} between two simplices in the new weak coupling phase, for $n = 3$ vector fields at $\kappa_2 = 4.5$ in a doubly logarithmic plot. The lines are the best linear fits to the data.

We consistently observe negative values $\gamma \approx -0.2$. This is in reasonable agreement with the prediction from the strong coupling expansion, $\gamma \approx -0.38$.

3.4.5 Discussion

The most interesting result is the discovery that matter fields can prevent the collapse of 4d simplicial manifolds to branched polymers. We find for the first time a strong back reaction of the matter on the geometry. The results suggest that when the number of vector-fields becomes larger than one the branched polymer phase disappears, and is replaced by a *new* phase with negative γ .

The numerical data does not allow to determine the order of the transition unambiguously. However for one vector field we observed indications for a first order transition but the latent heat of the transition is smaller compared to the jump observed for pure gravity. This may indicate that matter softens the transition. Therefore it is not excluded that with the correct mixture of matter-fields the transition is continuous.

The new weak coupling phase observed for three vector fields is very intriguing. The internal Hausdorff dimension is close to four, the same as for flat space. The negative γ values obtained numerically and with the strong coupling expansion indicate a non-trivial behavior. This is a very promising result because the negative γ may, like in two dimensions, indicate that the whole phase is critical and a non-trivial continuum limit can be taken. Gravitons, however, will presumably be present only if the Newton coupling is tuned to a critical value κ_2^c . If the transition found in our work is second order this induces infinite curvature-curvature correlations, which may be interpreted as gravitons.

Our results obtained numerically and with the series expansion support the conjecture in [52] mentioned in the introduction. As predicted we find that additional matter stabilizes the geometry as opposed to the case in two dimensions where matter de-stabilizes the surface.

After all it should, however, not be forgotten that one still faces some uncertainties. It is important to check carefully the nature of the transition. It should also be verified that the critical coupling in the thermodynamical limit is finite. In the weak coupling phase the curvature $N_0/N_4 \approx 0.25$ is close to the kinematic bound. The local volume $o(p) \propto N^{3/4}$ of the sub-singular vertices in this phase take no finite fraction of the whole volume in the thermodynamical limit, but the local volume still diverges.

3.5 Algorithm

The algorithm used to generate the data presented in this chapter uses the framework of dynamical Monte Carlo algorithms discussed in section (1.7). In this section we want to describe the transformations (1.54) and the weight (1.59) specific to the algorithm used to simulate four dimensional simplicial quantum gravity. We also discuss the weights induced by the vector field used in section 3.4.

In order to calculate the transition probabilities, remember that the distribution of manifolds T we want to generate is given by

$$p(T, \{A\}_T) \sim \exp -S_g[T] - S_A[T, \{A\}_T], \quad (3.43)$$

where the first term corresponds to the Einstein-Hilbert action. The action S_A of the matter field living on the manifold is given by

$$S_A[T, \{A\}_T] = \sum_{i=1}^n \sum_{t \in T} o(t) (A^{(i)}(l_{12}) + A^{(i)}(l_{23}) + A^{(i)}(l_{31}))^2. \quad (3.44)$$

The second sum runs over all triangles t of the triangulation T , $o(t)$ is the order of the triangle t , and l_{12}, l_{23}, l_{31} are the three oriented edges of t . The field A is an oriented link variable, which means $A(-l) = -A(l)$. Therefore the action is invariant under a gauge transformation at vertex p_0 : simultaneous translation $A(l) \rightarrow A(l) + \epsilon$ of all $A(l)$ living on links emerging from p_0 does not change the action. The first sum runs over the number of matter fields coupled to gravity. For the sake of simplicity, we discuss in the following only the case $n = 1$. The extension to $n > 1$ is straightforward.

The geometric moves $M_{(p,q)}$ which we describe in detail below may generate and destroy links and hence field variables $A(i)$. In principle one could update the geometry and the matter at the same time. A procedure would be to assign random values to new matter variables and accept or reject the whole transformation with a Metropolis weight. However, if one assigns the $A(l_i)$ with a flat distribution the efficiency is very low because then most transformations will be rejected in the Metropolis step. One might try to assign to the configuration A a Gibbs distribution

$$\pi_{(p,q)}(A) = \frac{e^{-S(A)}}{V(A)}, \quad (3.45)$$

with the normalization

$$V(A) = \int'_A \mathcal{D}A e^{-S_A(A)} \quad (3.46)$$

The integral runs over all accessible states of the new matter-fields. The prime indicates that we do not integrate over the zero-modes of the action. The probability can, however, not directly be used as a heat-bath probability because in the grand canonical moves the normalization constant $V(A)$ is different for a move and its inverse. Therefore our algorithm updates gravity and matter in two steps. In the first step the geometric part of the transformation is accepted or rejected independently of the state of the new matter fields, which are integrated out. In

the second step the fields which were created in the geometric update are set with a heat-bath probability.

The detailed balance condition for the probability $\Pi_{(p,q)}$ to accept the geometric move (p, q) at a certain location on the manifold A reads then

$$\frac{V(A)}{n_i} \Pi_{(p,q)}(A) e^{-S_g(A) - S_s(A)} = \frac{V(B)}{n'_i} \Pi_{(p,q)}(A) e^{-S_g(B) - S_s(B)}. \quad (3.47)$$

The term S_s is the action of the matter field without contributions from terms involving the new matter field. In the geometrical update S_s changes because the move changes the order $o(t)$ of some triangles on the simplicial manifold. The factor involving the n_i are present to balance the grand canonical fluctuations of the manifold. The $n_i, i = 3, 4, 5$ count the number of possible locations, where a local deformation can be applied. We have discussed this factor in detail in the context with expression (2.28) for the hyper-cubic random surface model.

The matter field is not only updated in the geometrical transformations. The algorithm switches between updates in the geometrical and the matter sector. In the matter update we choose an extensive number of links from the manifold. Each link is sequentially subjected to a heat-bath or an over-relaxation step. In the heat-bath, link field A on the link l_{12} is chosen from the distribution :

$$P(A) \sim \exp \left(- \sum_t o(t) (A - A_{1p} + A_{2p})^2 \right) = \exp (-\alpha(A - \beta/\alpha)^2) \quad (3.48)$$

where the sum runs over all triangles $t = t_{12p}$ which have the link l_{12} as an edge and the point p as a vertex. The variables α, β in the rightmost expression are defined by

$$\alpha = \sum_t o(t) \quad (3.49)$$

$$\beta = \sum_t o(t) (A_{1p} - A_{2p}). \quad (3.50)$$

The over-relaxation is a micro-canonical transformation

$$A \rightarrow -A + 2\beta/\alpha, \quad (3.51)$$

which does not change the action. This transformation is more efficient compared to the heat-bath in terms of mobility, however, the move is not ergodic. Therefore we have to mix the over-relaxation update with the heat-bath update.

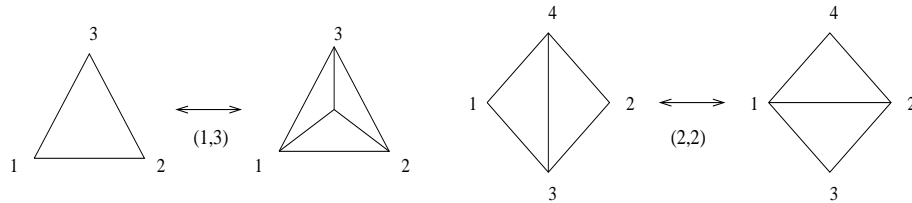


Figure 3.9: The (p, q) transformations in two dimensions

In the following sections we describe in detail the geometric transformations and the weights derived for the 5 (p, q) moves in four dimensions. For the transformations where new field variables are created we derive also the heat-bath probability for the fields. To clarify the notation for the geometric transformations, consider first the 3 (p, q) -transformations in two dimensions depicted in figure 3.9. We use the notation $tp_1p_2p_3$ to denote a triangle which contains the vertices with the labels p_1, p_2, p_3 . The first transformation $M_{(1,3)}$ inserts a vertex into a triangle. We write this as

$$t\underline{123} \leftrightarrow t\underline{124} + t\underline{134} + t\underline{234}. \quad (3.52)$$

The inverse transformation $M_{(3,1)}$ removes a vertex. With this procedure the number of triangles grows (decreases) by 2, the number of links grows (decreases) by 3 in the triangulation.

The second transformation $M_{(2,2)}$ flips a link:

$$t\underline{134} + t\underline{234} \leftrightarrow t\underline{123} + t\underline{124} \quad (3.53)$$

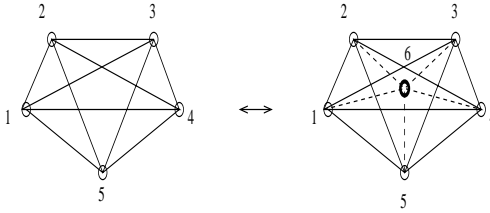
This transformation is self-dual. Using the transformation at the 'same' location twice does not change the geometry.

In the four dimensional case presented in the following sections we denote a four simplex $sp_1p_2p_3p_4p_5$ by enumerating the labels of the vertices p_i .

3.5.1 Move 15, 51

The move $M_{(1,5)}$ inserts a vertex p_6 into a four-simplex $s12345$. This step generates 4 four-simplices, 10 triangles, 5 links and, together with the links, five new field variables $A(li6) = x_i, i = 1, \dots, 5$.

$$s\underline{12345} \leftrightarrow s\underline{12346} + s\underline{12356} + s\underline{12456} + s\underline{13456} + s\underline{23456} \quad (3.54)$$



The change in the geometric part of the action is

$$\Delta S_g = 4\kappa_4 - 10\kappa_2. \quad (3.55)$$

The order $o(t)$ of the triangles $t \in s12345$ changes by +1. The "old" fields therefore contribute

$$\Delta S_s(A) = \sum (A_{ij} + A_{jk} + A_{ki})^2. \quad (3.56)$$

The sum runs over all triangles which change the order by +1 in the transformation $M_{(1,5)}$. The new fields contribute

$$S_A[x] = 3 \sum_{i,j,i < j} (A_{ij} + x_j - x_i)^2 \quad (3.57)$$

to the action. The sum runs over pairs $i < j \leq 5$ of the points of $s12345$. For the probability $\Pi_{(p,q)}$ (3.47) we have to calculate the volume $V(x)$ (3.46) for the new fields. We find

$$V = \int \frac{d^5x}{zero\ mode} e^{-S_a[x]} = \frac{\pi^2}{125} \exp \left(\frac{3}{5} \sum_{\langle ijk \rangle} (A_{ij} + A_{jk} + A_{ki})^2 \right) \quad (3.58)$$

With (3.47) we get for the Metropolis weight

$$\Pi_{(1,5)} = \min \left\{ 1, \frac{\pi^2}{125} \frac{n_4}{n_5'} e^{-\Delta S_g} \exp \left(-\frac{2}{5} \sum_{\langle ijk \rangle} (A_{ij} + A_{jk} + A_{ki})^2 \right) \right\} \quad (3.59)$$

for the geometrical part of the move.

The inverse transformation removes a suitable vertex from the simplicial manifold. No new fields are created and hence $V_b = 1$. The weight for this move is :

$$\Pi_{(5,1)} = \min \left\{ 1, \frac{125}{\pi^2} \frac{n_5}{n_4'} e^{\Delta S_g} \exp \left(\frac{2}{5} \sum_{\langle ijk \rangle} (A_{ij} + A_{jk} + A_{ki})^2 \right) \right\} \quad (3.60)$$

After the geometric part of the transformation $M_{(1,5)}$ has been accepted the five new link-variables $x_i = A(l_{i6})$ have to be assigned with a heat bath probability. One of them, say x_5 , may be set zero due to the gauge degree of freedom. The others are chosen with a Gaussian distribution :

$$\begin{aligned} P(x_1, x_2, x_3, x_4, x_5 = 0) &\sim \exp \left(-3 \sum_{i,j,i < j} (A_{ij} + x_j - x_i)^2 \right) \\ &\sim \exp \left(-3(x^T M x - 2w^T x) \right) \end{aligned} \quad (3.61)$$

where

$$M = \begin{bmatrix} 4 & -1 & -1 & -1 \\ -1 & 4 & -1 & -1 \\ -1 & -1 & 4 & -1 \\ -1 & -1 & -1 & 4 \end{bmatrix} \quad (3.62)$$

and

$$w_i = \sum_{j,j \neq i} A_{ij}. \quad (3.63)$$

It is convenient to diagonalize the symmetric matrix M to decouple the fields. Denote the components of the vector in the eigenvector bases by y_1, y_2, y_3, y_4 . The distribution for the y_i in this bases is given by

$$\begin{aligned} P(y_1) &\sim \exp(-3(y_1 - \Omega_1)^2) & \Omega_1 &= \frac{1}{2}(w_1 + w_2 + w_3 + w_4) \\ P(y_2) &\sim \exp(-15(y_2 - \Omega_2/5)^2) & \Omega_2 &= \frac{1}{2}(w_1 + w_2 - w_3 - w_4) \\ P(y_3) &\sim \exp(-15(y_3 - \Omega_3/5)^2) & \Omega_3 &= \frac{1}{\sqrt{2}}(w_1 - w_2) \\ P(y_4) &\sim \exp(-15(y_4 - \Omega_4/5)^2) & \Omega_4 &= \frac{1}{\sqrt{2}}(w_3 - w_4) \end{aligned} \quad (3.64)$$

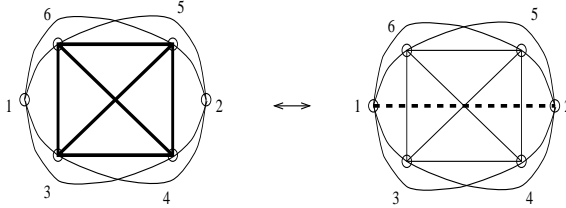
This assigns a random value to the y_i with the distribution given above. The new fields x_i are obtained by a base-transformation :

$$\begin{aligned} x_1 &= \frac{1}{2}(y_1 + y_2 + \sqrt{2}y_3) \\ x_2 &= \frac{1}{2}(y_1 + y_2 - \sqrt{2}y_3) \\ x_3 &= \frac{1}{2}(y_1 - y_2 + \sqrt{2}y_4) \\ x_4 &= \frac{1}{2}(y_1 - y_2 - \sqrt{2}y_4) \end{aligned} \quad (3.65)$$

3.5.2 Move 24, 42

The move $M_{(2,4)}$ inserts one new link into the manifold. This generates also four triangles and two four-simplices:

$$s\underline{13456} + s\underline{23456} \leftrightarrow s\underline{12345} + s\underline{12346} + s\underline{12356} + s\underline{12456} \quad (3.66)$$



The change in the geometric part of the action is :

$$\Delta S_g = 2\kappa_4 - 4kappa_2. \quad (3.67)$$

In the calculation of the volume V of the configuration space for the new field $x = A(l12)$ we use the notation (3.66): the new link $l12$ connects the vertices $p1$ and $p2$, the simplices $s13456$ and $s23456$ have a common tetrahedron $T3456$. The order of the four triangles $t \in T3456$ decrease by 1 in the move $M_{(2,4)}$ while the orders of the remaining 12 triangles in $s13456$ and $s23456$ increase by 1.

Denote by

$$P_{ijk} = (A_{ij} + A_{jk} + A_{ki})^2 \quad (3.68)$$

the value of the plaquette P_{ijk} . One gets the following change in the action for the "old" fields :

$$\Delta S_s(A) = - \sum_{3 \leq i < j < k \leq 6} P_{ijk} + \sum_{2 < i < j \leq 6} (P_{1ij} + P_{2ij}) \quad (3.69)$$

The volume of the state space for the new field is

$$V = \sqrt{\frac{\pi}{12}} \exp -3 \sum_{j=3}^6 (A_{1j} + A_{j2})^2. \quad (3.70)$$

Collecting these results together one finds for the transition probability

$$\Pi_{(2,4)} = \min \left\{ 1, \frac{n_{14}}{n'_3} \times V \times e^{-\Delta S_g - \Delta S_s} \right\} \quad (3.71)$$

and

$$\Pi_{(4,2)} = \min \left\{ 1, \frac{n_{14}}{n'_3} \times V^{-1} \times e^{\Delta S_g + \Delta S_s} \right\} \quad (3.72)$$

for the inverse move $M_{(4,2)}$.

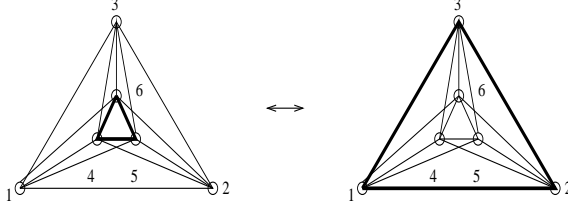
The heat-bath weight for the one new field is given by eq. (3.48).

3.5.3 Move 33

This move flips a triangle on the manifold. The transformation is self-dual and does not change the number of (sub)-simplices. Therefore we do not have to deal with a new field:

$$V = 1. \quad (3.73)$$

$$s12456 + s13456 + s23456 \leftrightarrow s12345 + s12346 + s12356 \quad (3.74)$$



In the transition probability one has to take into account the change ΔS_s coming from the change of $o(t)$. From 3.74 one can read off

$$\Delta S_s(A) = \sum_{i,j=1, i \neq j}^3 \sum_{k=4}^6 (A_{ij} + A_{jk} - A_{ki})^2 - \sum_{j,k=1, j \neq k}^3 \sum_{i=4}^6 (A_{ij} + A_{jk} - A_{ki})^2. \quad (3.75)$$

The action of the gravity sector is unchanged. Therefore the transition probability for the geometric part of the move is

$$\Pi_{(3,3)} = \min \left\{ 1, \frac{n_3}{n'_3} \times e^{-\Delta S_s} \right\} \quad (3.76)$$

Chapter 4

Summary

In this thesis we have analyzed two different models of random geometries, namely hyper-cubic random surfaces and four dimensional simplicial quantum gravity. Although these models are different, e.g. the local dimension of the models considered is two and four respectively, they have common properties. For example both models possess a branched polymer phase. The appearance of this phase, however, is often referred to as a 'collapse to triviality' because the basically one dimensional structure does not describe extended d -dimensional ($d = 2, 4$) geometries in the continuum limit. One problem we addressed for both models was therefore to find modifications of the models with a different critical behavior. In both cases we find such modifications.

The hyper-cubic random surface model is a discretization of bosonic strings embedded in a D -dimensional space. In three dimensions the model can also be interpreted as a fluid membrane. We have analyzed the phase diagram of the model with an extrinsic curvature term in the action. Numerically we find two phases in three and four dimensions: a weak coupling phase with a branched polymer behavior and a flat strong coupling phase. The Hausdorff dimension is $d_h = 4$ in the branched polymer phase and $d_h = 2$ in the flat phase. The transition is of first order, the critical coupling is finite. We have shown that the existence of this transition is not in contradiction with an earlier renormalization group analysis of the model, which under some assumptions indicated that the model is always in the branched polymer phase for finite coupling to the external curvature. One cannot take the continuum limit at the transition point because the transition is of first order. One can, however, try to smoothen this transition by introducing self-avoidance into the model. This is motivated by the observation that for the related model of Ising spins with a gonihedric action without self-avoidance of the dual surfaces evidence for a first order and with weak self-avoidance evidence for a second order phase transition was found [44, 45].

We have solved an old question concerning the hyper-cubic random surface model. Earlier investigations indicated that the model with a certain local constraint has a different critical behavior compared to the unrestricted model. We have shown that this is not the case. The true behavior of the constrained model is masked by very strong finite size effects. In the thermodynamical limit the constrained and the unconstrained model have the same critical behavior. This shows

the universality of the model in the sense that the behavior of the model does not depend on details of the discretization.

For the model of four dimensional simplicial quantum gravity we found that coupling more than two gauge vector fields to gravity suppresses the branched polymer phase. Our numerical data and a strong coupling expansion indicate that the branched polymer phase is replaced by a new phase of gravity. The Hausdorff dimension in this phase is close to four, the dimension of flat space. We find a negative entropy exponent γ in this phase. This may indicate, similar to the model in two dimensions, that the whole phase is critical so that one can take a non-trivial continuum limit. One can hope to find gravitons in this model at the phase transition if the transition is of second order. However, the statistics of our numerical data does, at the moment, not allow to determine its order. Our ongoing numerical investigations of the model therefore concentrate on the nature of the phase transition. In the future the geometrical properties of the dominating manifolds at the transition point and in the new phase have to be analyzed. This will allow to answer the question of whether the dominating geometries describe, on large scales, a flat four-dimensional Euclidean space-time. If this is the case, we may have succeeded in finding a stable ground state of four dimensional euclidean quantum gravity. The observation that matter is required to stabilize the ground state of quantum gravity would then suggest that matter may be required for the very existence of a stable universe.

A different question which we addressed for four dimensional quantum gravity concerns the role of topological excitations. It is not a priori clear whether topological excitations should be taken into account in this model. We have checked numerically for three different topologies whether topological excitations are exponentially suppressed in the thermodynamical limit. We have shown that the leading contribution to the free energy does not depend on the topology and hence the topological excitations survive in the thermodynamical limit. This result supports the conjecture that it is possible to define the model with coherent contributions from all topological excitations at a double scaling limit similar to the two dimensional model.

4.1 Acknowledgement

I want to thank Prof. B. Petersson for proposing such an interesting research activity. Without his guidance, technical and academic advice and patience this thesis would never have been possible. It is a pleasure to thank Z. Burda, G. Thorleifsson and J. Tabaczek for the long and fruitful discussions we have had in the recent years. I am grateful to the HLRZ Jülich for computer time on PARAGON. The HRZ Bielefeld supported me by supplying computer hardware for a Pentium farm, which I used to perform large parts of the numerical calculations.

Bibliography

- [1] J. Polchinsky, *What is String Theory ?*, Proc. Les Houches Summer School, Session LXII (1994) 287.
- [2] L. Peliti, *Amphiphilic Membranes in fluctuating geometries in statistical mechanics and field theory*, Les Houches Summer School (1994) 195.
- [3] D. R. Nelson, *Defects in Superfluids, Superconductors and Membranes in fluctuating geometries in statistical mechanics and field theory*, Les Houches Summer School (1994) 423.
- [4] V. Knizhnik, A. Polyakov, A. Zamolodchikov, Mod. Phys. Lett A3 (1988) 819-
- [5] P. Ginsparg, *Matrix Models of 2d Gravity* Trieste HEP Cosmol. 1991, 785 (hep-th/9112013)
- [6] J. Ambjørn, *Quantization of geometry in fluctuating geometries in statistical mechanics and field theory*, Proc. Les Houches Summer School (1994) 77.
- [7] J. Ambjørn, B. Durhuus, T. Jonsson, J. Phys. A21 (1977) 981.
- [8] J. Ambjørn, B. Durhuus, T. Jonsson, Europhys. Lett. 3 (1987) 1059.
- [9] A.M. Polyakov, *Gauge Fields and Strings*, Harwood Academic Publishing (1987).
- [10] T. Morris, Nucl. Phys. B341 (1990) 443.
- [11] L.D. Landau, E.M. Lifschitz *Lehrbuch der theoretischen Physik, Band II*. Akademie-Verlag Berlin (1939).
- [12] S. Weinberg, *Gravitation and Cosmology: Principles and applications of the general theory of relativity*, Wiley (1971).
- [13] J.B. Hartle, S.W. Hawking, Phys. Rev. D28 (1983) 2690.
- [14] J. Ambjørn, B. Durhuus, J. Fröhlich, Nucl. Phys. B257 (1985) 433
- [15] F. David, Nucl. Phys. B257 (1985) 45 F. David, Nucl. Phys. B257 (1985) 543
- [16] V. A. Kazakov, Phys. Lett. B150 (1985) 182.
- [17] V. A. Kazakov, Mod. Phys. Lett. A4 (1989) 2125.

- [18] M.L. Mehta, Comm. Math. Phys. 79 (1981) 327.
- [19] E. Brezin, V.A. Kazakov, Phys. Lett. B236 (1990) 144.
- [20] M. Douglas, S. Shenker, Nucl. Phys. B335 (1990) 635.
- [21] D. Gross, A.A. Migdal, Phys. Rev. Lett. 64 (1990) 127.
- [22] V.A. Kazakov, Phys. Lett. A119 (1986) 140.
- [23] J. Ambjørn, B. Durhuus, J. Fröhlich, P. Orland, Nucl. Phys. B257 (1985) 433; B270 (1986) 457; B275 (1986) 161
- [24] D. Weingarten, Phys. Lett. B90 (1980) 280.
- [25] B. Durhuus, J. Fröhlich, T. Johnsson, Nucl. Phys. B240 (1980) 453
- [26] B. Baumann, B. Berg, Phys. Lett. B164 (1985) 131
B. Baumann, B. Berg, G. Münster, Nucl. Phys. B305 (1988)
- [27] B. Petersson, G. Thorleifsson, *Beyond the $C = 1$ barrier in two dimensional quantum gravity* (hep-lat/9710077).
- [28] F. David, Nucl. Phys. B487 (1997) 633.
- [29] J. Ambjørn, Nucl. Phys. Proc. Suppl. 42 (1995) 3.
- [30] B. Durhuus, Nucl. Phys. B426 (1994) 203.
- [31] J. Ambjørn, S. Jain, G. Thorleifsson, Phys. Lett. B307 (1993).
- [32] S. Jain, S. Mathur, Phys. Lett. B286 (1992) 239.
- [33] B. Durhuus, T. Jonsson Phys. Lett. B140 (1986) 385.
- [34] A.M. Ferrenberg, R.H. Swendsen, Phys. Rev. Lett. 61 (1988) 2635.
- [35] B. Berg, A. Billoire, D. Foerster, Nucl. Phys. B251 (1985) 665
B. Baumann, Nucl. Phys. B285 (1987) 391
- [36] J. Ambjørn, A. Irback, J. Jurkiewicz, B. Petersson, Nucl. Phys. B 393 (1993) 571.
- [37] M. Bowick, P. Coddington, L. Han, G. Harris, E. Marinari Nucl. Phys. B394 (1993) 791.
- [38] K. Anagnostopoulos, M. Bowick, P. Coddington, M. Falcioni, L. Han, G. Harris, E. Marinari, Phys. Lett. B317 (1993) 102.
- [39] W. Helfrich, J. Naturforsch. C28 (1973) 693.
- [40] A. M. Polyakov, Nucl. Phys. B268 (1986) 406.
- [41] H. Kleinert, Phys. Lett. A114 (1986) 263.

- [42] D. Forster, Phys. Lett. A114 (1986) 115.
- [43] G.K. Savvidy, F.J. Wegner Nucl. Phys. B413 (1994) 605.
- [44] D. Espriu, M. Baig, D.A. Johnston, R.P.K.C. Malmini Phys. A30 (1997) 405.
- [45] D.A. Johnston, R.P.K.C. Malmini, Nucl. Phys. Proc. Suppl. 53 (1997) 773.
- [46] T. Eguchi, H. Kawai, Phys. Lett. B114 (1982) 247.
- [47] A. M. Polyakov, Phys. Lett. B59 (1975) 79.
- [48] S. Weinberg, in *General Relativity, an Einstein centenary survey* S.W. Hawking, W. Israel (Edts.), Cambridge University Press (1979).
- [49] H. Kawai, N. Ninomiya, Nucl. Phys. B336 (1990) 115.
- [50] P. Bialas, Z. Burda, A. Krzywicki, B. Petersson, Nucl. Phys. B472 (1996) 293.
- [51] B. V. de Bakker Phys. Lett. B389 (1996) 238
- [52] I. Antoniadis, P.O. Mazur and E. Mottola, Phys. Lett. B394 (1997) 49.
- [53] M.E. Agishtein, A.A. Migdal, Mod. Phys. Lett. A6 (1991) 1863.
- [54] M.E. Agishtein, A.A. Migdal, Nucl. Phys. B385 (1992) 395.
- [55] J. Ambjørn, J. Jurkiewicz, Phys. Lett. B278 (1992) 42
- [56] D.M.Y. Sommerville, Proc. Roy. Soc. Lond. A115 (1927) 103.
- [57] F. David *Simplicial Quantum Gravity and Random Lattices*, Proc. Les Houches Sum. Sch. 92 (1992) 679.
- [58] J. Ambjørn, J. Jurkiewicz, C. F. Kristjansen, Nucl. Phys. B393 (1993) 601.
- [59] S. Catterall, J. Kogut and R. Renken, Phys. Rev. Lett 72 (1994) 4062.
- [60] J. Ambjørn, J. Jurkiewicz, Phys. Lett. B335 (1994) 355.
- [61] B. Brugmann, E. Marinari, Phys. Lett. B349 (1995) 35.
- [62] C. Bartocci, U. Bruzzo, M. Carfora, A. Marzuoli, J. Geom. Phys. 18 (1996) 247.
- [63] S. Catterall, J. Kogut, R. Renken
- [64] J. Ambjørn, Z. Burda, J. Jurkiewicz and C.F. Kristjansen, Phys. Lett. **B297** (1992) 253; Phys. Rev. D48 (1993) 3695;
- [65] J. Ambjørn, S. Bilke, Z. Burda, J. Jurkiewicz and B. Petersson, Mod. Phys. Lett. A9 (1994) 2527;
- [66] S.M. Catterall, J.B. Kogut and R.L. Renken, Nucl. Phys. **B389** (1993) 601; Nucl. Phys. B422 (1994) 677.

- [67] T. Hotta, T. Izubuchi, J. Nashimura, *Prog. Theor. Phys.* 94 (1995) 263.
- [68] S. Catterall, G. Thorleifsson, J. Kogut, R. Renken, *Nucl. Phys.* B468 (1996) 263.
- [69] P. Bialas, Z. Burda and D. Johnston, *Nucl. Phys.* B493 (1997) 505.
- [70] P. Bialas, Z. Burda *Collapse of 4-D random geometries* (hep-lat/9707028).
- [71] P. Bialas, Z. Burda, B. Petersson, J. Tabaczek, *Nucl. Phys.* B495 (1997) 463.
- [72] J. Tabaczek, M. Sc. Thesis, University of Bielefeld 1997
- [73] S. Catterall, R. Renken, J. Kogut, (hep-lat/9709007)
- [74] J. A. Wheeler, *Geometrodynamics and the issue of the final state*, in *Relativity, Groups & Topology*, eds. B.S. DeWitt and C.M. DeWitt (Blackie and Son Ltd., Glasgow, 1964) 317
- [75] S.W. Hawking, *Nucl. Phys.* B144 (1978) 349.
- [76] B. V. de Bakker, *Nucl. Phys. Proc. Suppl.* 42 (1995) 716.
- [77] M. Gross, S. Varsted, *Nucl. Phys.* B378 (1992) 367
- [78] P. Bialas, *Correlations in fluctuating geometries*, *Nucl. Phys. Proc. Suppl.* 53 (1997) 739
- [79] S. Catterall, R. Renken, J. Kogut, *Phys. Rev. Lett.* 72 (1994) 4062
- [80] J. Ambjørn and J. Jurkiewicz, *Phys. Lett.* B335 (1994) 355.
- [81] B. Brüggmann and E. Marinari, *Phys. Lett.* B349 (1995) 35.
- [82] M.E. Cates, *Europhys. Lett.* 8 (1988) 719.
- [83] A. Krzywicki, *Phys. Rev.* D41 (1990) 3086.
- [84] F. David, *Nucl. Phys.* B368 (1992) 671.
- [85] V.I. Brezinskii, *Zh. Eksp. Teor. Fiz.* 59 (1970) 907 [*Soviet Physics, JETP* 32 (1971) 493].
- [86] M. Kosterlitz, D. Thouless, *J. Phys.* C6 (1973) 1181
- [87] J. Jurkiewicz and A. Krzywicki, *Phys. Lett.* B392 (1997) 291.
- [88] I. Antoniadis and E. Mottola, *Phys. Rev.* D45 (1992) 2013;
- [89] I. Antoniadis, P.O. Mazur and E. Mottola, *Nucl. Phys.* B388 (1992) 627.
- [90] F. David, J. Jurkiewicz, A. Krzywicki and B. Petersson, *Nucl. Phys.* B290 (1987) 218.
- [91] J. Ambjørn and J. Jurkiewicz, *Nucl. Phys.* B451 (1995) 643.

- [92] S. Catterall, J. Kogut, R. Renken, G. Thorleifsson, Phys. Lett. B 366 (1996)
72